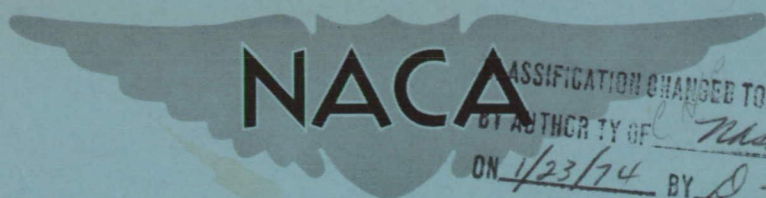


~~CONFIDENTIAL~~

Copy
RM L52G31

e-1



NACA

CLASSIFICATION CHANGED TO Unclass
BY AUTHORITY OF Naval TD-73-403
ON 1/23/74 BY D. Harkweather

RESEARCH MEMORANDUM

CALIBRATION OF STRAIN-GAGE INSTALLATIONS IN AIRCRAFT
STRUCTURES FOR THE MEASUREMENT OF FLIGHT LOADS

By T. H. Skopinski, William S. Aiken, Jr.,
and Wilber B. Huston

Langley Aeronautical Laboratory
Langley Field, Va.

ENGINEERING DEPT. LIBRARY
CHANCE-VOUGHT AIRCRAFT
DALLAS, TEXAS

CLASSIFIED DOCUMENT

This material contains information affecting the National Defense of the United States within the meaning of the espionage laws, Title 18, U.S.C., Secs. 793 and 794, the transmission or revelation of which in any manner to unauthorized person is prohibited by law.

NATIONAL ADVISORY COMMITTEE FOR AERONAUTICS

WASHINGTON

October 8, 1952

~~CONFIDENTIAL~~

001 22 1982

NATIONAL ADVISORY COMMITTEE FOR AERONAUTICS

RESEARCH MEMORANDUM

CALIBRATION OF STRAIN-GAGE INSTALLATIONS IN AIRCRAFT
STRUCTURES FOR THE MEASUREMENT OF FLIGHT LOADS

By T. H. Skopinski, William S. Aiken, Jr.,
and Wilber B. Huston

SUMMARY

A general method has been developed for calibrating strain-gage installations on aircraft structures, which permits the measurement in flight of the shear or lift, the bending moment, and the torque or pitching moment on the principal lifting or control surfaces. Although the stress in structural members may not be a simple function of the three loads of interest, a straightforward procedure is given for numerically combining the outputs of several bridges in such a way that the loads may be obtained. Extensions of the basic procedure by means of electrical combination of the strain-gage bridges are described which permit compromises between strain-gage installation time, availability of recording instruments, and data reduction time. The basic principles of strain-gage calibration procedures are illustrated by reference to the data for two aircraft structures of typical construction, one a straight and the other a swept horizontal stabilizer.

INTRODUCTION

The measurement of loads on aircraft in flight is required for a variety of purposes such as in research investigations, structural integrity demonstrations, and developmental flight testing. Although pressure-distribution methods permit the determination of aerodynamic loads without corrections for inertia effects, pressure installations must be very complete in order that accurate load data may be obtained. Since the time of installation and data reduction may be lengthy, the general use of pressure-distribution methods in the measurement of loads on aircraft in flight is avoided except when specific detailed load-distribution data are desired.

A more useful tool for the measurement of the over-all loads on aircraft structures appears to be the wire resistance strain gage. Properly

installed and calibrated, such gages may be used to determine the structural loads on control surfaces, landing-gear structures, and relatively complex built-up wing and empennage assemblies. The measured structural loads can, in turn, be converted to aerodynamic loads provided the structural weight distribution is known and the acceleration distribution has been measured.

References 1 to 5 illustrate various strain-gage calibration techniques, certain elements of which are common to a general method which has been used successfully in flight loads research by the National Advisory Committee for Aeronautics since 1944; references 6 to 9 contain typical flight loads data obtained by the application of this general method. Because of the increased interest in strain-gage methods, and in an attempt to resolve some of the difficulties which are being encountered in the use of strain gages for flight loads measurements, the present paper is being published.

In this paper a basic calibration procedure is developed for calibrating strain-gage installations on aircraft structures which permits the measurement in flight of the shear, bending moment, and torque. Extensions of the basic procedure by use of electrical combination of strain-gage bridges are described which permit compromises between strain-gage installation time, availability of recording instruments, and data reduction time for flight measurements. Since many of the elements of the calibration procedure are best illustrated by reference to and use of experimental data, this paper also includes calibration data and analysis procedures used for two typical aircraft structures. One of these, structure A, is the horizontal stabilizer of the airplane for which tail load measurements are given in references 8 and 9. In addition, three other calibration procedures of very limited application are briefly discussed in an appendix.

SYMBOLS

L_p	general symbol for shear, bending moment, or torque (see eq. (40))
M	bending moment, in.-lb
T	torque, lb-in.
V	shear, lb

Note: Prime (') denotes applied values of calibrate loads.

Additional subscripts pertaining to M, T, and V or M', T' and V':

L	left
R	right
j	number of applied loads for exact simultaneous-equation solutions
n	number of applied loads for least-squares solutions
a_{ij}	preliminary load coefficient for structure A
b_{ij}	preliminary load coefficient for structure B
a'_{ij}	final load coefficient for structure A
b'_{ij}	final load coefficient for structure B
k_1, k_2	constants in equation (34)
m_{ij}	element of inverse matrix
x	distance from torque reference line, in.
x^r	general term for nonlinear chord position effect
y	distance perpendicular to center line outboard of strain-gage station, in.
y_Δ	distance along sweep axis outboard of strain-gage station, in.
y^s	general term for nonlinear span position effect
α_{ij}	constant in influence coefficient equation
β_{ij}	constant in load equation
δ	deflection of galvanometer in strain-gage circuit
δ_{\max}	calculated galvanometer deflection given by equation (35)
δ_{cal}	deflection of galvanometer in strain-gage circuit due to shunting of calibrate resistor across one arm of the strain-gage bridge

ϵ_V	residual, difference between calculated and applied shear
μ	nondimensional bridge response, $\delta_{\max}/\delta_{\text{cal}}$
μ_i	nondimensional response of the i^{th} uncombined strain-gage bridge ($i = 1, 2, 3, \dots, j$)
μ_{ij}	nondimensional response of the j^{th} uncombined strain-gage bridge due to the i^{th} applied calibrate load (exact solution, $i = 1, 2, 3, \dots, j$)
μ_{nj}	nondimensional response for the j^{th} uncombined strain-gage bridge due to the n^{th} applied calibrate load (least-squares solution, $n > j$)
μ_V	nondimensional response of an uncombined shear bridge
μ_M	nondimensional response of an uncombined bending-moment bridge
μ_T	nondimensional response of an uncombined torque bridge

Additional subscripts for μ :

Second subscript:

L left side
 R right side
 F front spar
 M mid spar
 R rear spar
 FT front top
 FB front bottom
 RT rear top
 RB rear bottom

Third subscript:

1 strain-gage station 1

2 strain-gage station 2

Example: μ_{VLF_1} designates the nondimensional response of an uncombined shear bridge mounted on the left front spar at strain-gage station 1

ρ nondimensional response for electrically combined bridges,
 $\delta_{\max}/\delta_{\text{cal}}$

Note: Subscripts for ρ are the same as for μ except that spar location of combined bridges is not required.

Matrix symbols:

$[\]$ square matrix

$\| \|$ rectangular matrix

$\| \|^T$ transpose of rectangular matrix

$[\]$ row matrix

$\{ \}$ column matrix

$[\]^{-1}$ inverse matrix

$| [\] |$ determinant of matrix

i row index

j column index

BASIC PROCEDURES FOR CALIBRATION

General Considerations

Although the use of the wire resistance strain gage for loads measurements is in some respects similar to its use in stress determination, a somewhat different approach is required since strain is to be used only as a means of obtaining information about the loads. In stress measurement, a single strain gage is usually used to determine the stress in a member. In loads measurement, four-active-arm bridges are generally applied on the principal structural members in order to obtain higher sensitivity and relative freedom from the effects of uniform structural temperature changes.

In flight research the loads of primary interest are generally those on wing or tail surfaces, and, in order to simplify the exposition of the procedures in this paper, descriptions are generally given in terms of a cantilever structure such as a wing or tail. The methods may, however, be utilized with other structures.

The first step in the measurement of flight loads by means of strain gages is a selection of the gage location, which depends on the measurements to be made. It is necessary to locate the gages at positions where the stress levels will be adequate to obtain good sensitivity and, at the same time, be away from areas of local stress concentrations. A typical installation is illustrated in figure 1(a), where four-active-arm bridges are shown installed on a typical two-spar structure. Ideally, it would be desirable to place the gages at a position such that a shear bridge would respond only to shear, and, as in reference 1, a moment bridge only to moment, and so forth, but generally it is only in an elementary truss type of beam that locations can be found where such a simple relationship between load and strain exists.

The loads on a surface such as an airplane wing can be completely specified by three orthogonal forces (normal, chord, and end force) and by three orthogonal moments (beam bending moment, torque, and chord bending moment). The strain in a given structural member can, therefore, be expected to be some function of these six quantities, and this strain response must be taken into account in any scheme which relates bridge output to applied load. Such a scheme should also allow for the fact that, with a complex structure such as a wing or tail, the stress in a root member may be affected not only by the loads outboard of the bridge station but also by loads on the opposite side or inboard of the strain-gage station. This carry-over effect can be of significance with unsymmetrical loading conditions. Certain simplifications are possible, however, since the end force on wings can be neglected, and the effects of chord forces will be negligible for the types of strain-gage installation.

shown in figure 1. For a wing structure which obeys Hooke's law, the stress in a member and, therefore, the output of a strain gage mounted on that member may be taken as some function of the three principal terms pertinent to aerodynamic loads investigations, the lift or shear, the bending moment, and the pitching moment or torque.

Development of Equations

The simplest relation between the output μ of a strain-gage bridge and the loads (shear, moment, and torque) on a panel outboard of that bridge can be expressed by the linear equation

$$\mu_i = \alpha_{i1}V + \alpha_{i2}M + \alpha_{i3}T \quad (1)$$

In the presence of carry-over, an expansion of this relation would be necessary in order to include the response of the bridge to loads applied on the opposite side or inboard of the bridge station. Such additional terms are introduced where necessary in the section entitled "Application of procedures."

The loads in equation (1) need not represent loads distributed over the entire area outboard of the strain-gage station provided the structure conforms to the principle of superposition; that is, the strain at a particular location due to loads applied simultaneously to several points on the structure is the algebraic sum of the strains due to the same loads applied individually. In this case, the load in equation (1) could be a load with a shear value V applied at some point with coordinates x, y . Thus the load would have bending moment and torque values given by

$$\begin{aligned} M &= Vy \\ T &= Vx \end{aligned} \quad (2)$$

in which case equation (1) can be rewritten as

$$\frac{\mu_i}{V} = \alpha_{i1} + \alpha_{i2}y + \alpha_{i3}x \quad (3)$$

Equation (3) implies that bridge output is proportional to the applied shear V and also that the relation between the output and the

coordinates of the point of application (x,y) is linear. Although the two types of linearity represented by equation (3) are rather severe restrictions, certain calibration procedures have essentially been based on this equation, and are treated briefly in the appendix. In the general case, equation (3) is not adequate. Although structures have usually followed Hooke's law, additional terms involving other than the first power of the coordinates are required if an explicit expression for bridge response is to be written. Nonetheless, equation (3) is useful in evaluating the performance of a bridge, if loads are applied at a number of points on the surface, and the bridge output expressed as μ/V is plotted against the y coordinate of the point of application with x as an independent parameter. Shear sensitivity is represented on such a plot by the intercept (equal to α_{i1}) when $x = y = 0$. Bending-moment sensitivity is shown by the slope α_{i2} of a plot of μ/V against y for a constant value of x, whereas torque response is represented by the variation of μ/V with x at constant values of y. The value of μ/V thus represents a sort of strain-gage influence coefficient, and since it represents the influence on the bridge output of a load at a given point, plots of μ/V against x and y are termed "influence-coefficient plots." Curvature in these plots for loads applied along any straight line on the structure indicates the necessity of including additional terms in the bridge-response equation. Although the form of these additional terms could perhaps be specified on theoretical grounds for some structures, it is shown that it is not necessary to know explicitly what these additional terms are.

An extension of equation (3) which includes additional terms involving the coordinates and which could apply to any of the bridges located in the structure is

$$\begin{aligned} \mu_i = & \alpha_{i1}V + \alpha_{i2}Vy + \alpha_{i3}Vx + \alpha_{i4}Vxy + \\ & \alpha_{i5}Vx^2 + \alpha_{i6}Vy^2 + \dots + \alpha_{ij}Vx^r y^s \end{aligned} \quad (4)$$

A calibration procedure can be evolved which allows for the presence of the additional terms by establishing relationships between applied load and the outputs of a number of bridges. The basis of this procedure and its application are illustrated in the equations which follow.

When bridges exhibit responses which can be represented by equation (4), with a finite number of terms (say j) then equations may be

written to relate the applied shear and its point of application to the output of each of j bridges as follows:

$$\left. \begin{aligned}
 \mu_1 &= \alpha_{11}V + \alpha_{12}V_y + \alpha_{13}V_x + \alpha_{14}V_{xy} + \dots + \alpha_{1j}V_x^r y^s \\
 \mu_2 &= \alpha_{21}V + \alpha_{22}V_y + \alpha_{23}V_x + \alpha_{24}V_{xy} + \dots + \alpha_{2j}V_x^r y^s \\
 \mu_3 &= \alpha_{31}V + \alpha_{32}V_y + \alpha_{33}V_x + \alpha_{34}V_{xy} + \dots + \alpha_{3j}V_x^r y^s \\
 &\vdots \\
 &\vdots \\
 &\vdots \\
 \mu_j &= \alpha_{j1}V + \alpha_{j2}V_y + \alpha_{j3}V_x + \alpha_{j4}V_{xy} + \dots + \alpha_{jj}V_x^r y^s
 \end{aligned} \right\} \quad (5a)$$

These equations are expressed in matrix form as

$$\left\{ \begin{array}{c} \mu_1 \\ \mu_2 \\ \mu_3 \\ \vdots \\ \vdots \\ \vdots \\ \mu_j \end{array} \right\} = \begin{bmatrix} \alpha_{11} & \alpha_{12} & \alpha_{13} & \dots & \alpha_{1j} \\ \alpha_{21} & \alpha_{22} & \alpha_{23} & \dots & \alpha_{2j} \\ \alpha_{31} & \alpha_{32} & \alpha_{33} & \dots & \alpha_{3j} \\ \vdots & \vdots & \vdots & \dots & \vdots \\ \vdots & \vdots & \vdots & \dots & \vdots \\ \alpha_{j1} & \alpha_{j2} & \alpha_{j3} & \dots & \alpha_{jj} \end{bmatrix} \left\{ \begin{array}{c} V \\ V_y \\ V_x \\ \vdots \\ \vdots \\ \vdots \\ V_x^r y^s \end{array} \right\} \quad (5b)$$

or

$$\{\mu\} = [\alpha] \{V_x^r y^s\} \quad (5c)$$

Equations (5) express the output of a number of bridges as a linear function of an equal number of terms of the type $V_x^r y^s$. The inverse



relation is therefore true that the loads can be expressed as a linear function of the outputs of j bridges, or

$$\{v_x^r y^s\} = [\beta] \{\mu_j\} \quad (6)$$

where

$$[\beta] = [\alpha]^{-1} \quad (7)$$

The necessary mathematical condition for the existence of a solution for the β coefficients of equation (6) is that the determinant of the α coefficients of equations (5) shall not vanish, that is

$$|[\alpha]| \neq 0 \quad (8)$$

This condition means that the j strain-gage bridges must have different characteristics, that is, the values of α for each bridge must not be linearly related to the values of α for the other bridges. If this solution exists, it is not necessary to know the values of the constants α_{ij} in the influence-coefficient equations (5) since the load coefficients β_{ij} in the load equations (6) could be determined by a suitable procedure. The primary purpose of the procedure, however, is to establish relationships between bridge response and the three loads, shear, moment, and torque. It is therefore not necessary to evaluate all of the β coefficients in equation (6) but only the values of the coefficients in the first three rows, that is:

$$\begin{Bmatrix} V \\ M \\ T \end{Bmatrix} = \begin{vmatrix} \beta_{11} & \beta_{12} & \beta_{13} & \dots & \beta_{1j} \\ \beta_{21} & \beta_{22} & \beta_{23} & \dots & \beta_{2j} \\ \beta_{31} & \beta_{32} & \beta_{33} & \dots & \beta_{3j} \end{vmatrix} \begin{Bmatrix} \mu_1 \\ \mu_2 \\ \mu_3 \\ \vdots \\ \mu_j \end{Bmatrix} \quad (9)$$



If these coefficients can be established, then equation (9) could be used for the determination of loads in flight from strain-gage responses.

The coefficients $\beta_{11} \dots \beta_{1j}$ in the equation for shear

$$V = \begin{bmatrix} \beta_{11} & \beta_{12} & \beta_{13} & \dots & \beta_{1j} \end{bmatrix} \begin{Bmatrix} \mu_1 \\ \mu_2 \\ \mu_3 \\ \vdots \\ \mu_j \end{Bmatrix} \quad (10a)$$

or transposed as

$$V = \begin{bmatrix} \mu_1 & \mu_2 & \mu_3 & \dots & \mu_j \end{bmatrix} \begin{Bmatrix} \beta_{11} \\ \beta_{12} \\ \beta_{13} \\ \vdots \\ \beta_{1j} \end{Bmatrix} \quad (10b)$$

can be determined if a number of known loads with shear values V'_1 to V'_j are applied to the structure. In view of equation (4) these loads must be applied at various chordwise and spanwise locations. If the number of applied loads is equal to the number of bridges j , then these loads and the bridge outputs can be written as

$$\begin{Bmatrix} V'_1 \\ V'_2 \\ \vdots \\ V'_j \end{Bmatrix} = \begin{bmatrix} \mu_{11} & \mu_{12} & \dots & \mu_{1j} \\ \mu_{21} & \mu_{22} & \dots & \mu_{2j} \\ \vdots & \vdots & \ddots & \vdots \\ \mu_{j1} & \mu_{j2} & \dots & \mu_{jj} \end{bmatrix} \begin{Bmatrix} \beta_{11} \\ \beta_{12} \\ \vdots \\ \beta_{1j} \end{Bmatrix} \quad (11a)$$



or

$$\{v'\} = [\mu] \{\beta\} \quad (11b)$$

and the coefficients $\{\beta\}$ can be determined from the solution of the simultaneous equations, or since matrix inversion is equivalent to solution of the simultaneous equations,

$$\{\beta\} = [\mu]^{-1} \{v'\} \quad (12)$$

In general, the number of bridges required in equations (5), and thus in equations (9), (10), and (11) is not known in advance, and therefore the exact number of calibrate loads required cannot be specified. If j bridges are available, all of which might be required, then n calibrate loads can be applied where $n > j$, and the values of the load coefficients $\beta_{11} \dots \beta_{1j}$ can be obtained by least-squares procedures. Such a solution involves calculation of the least-squares normal equations and solution of the resulting simultaneous equations. These steps can be represented conveniently as a series of matrix operations. The responses μ_{nj} of j bridges to each of n applied loads would be related to the shear values of these loads $v'_1 \dots v'_n$ by the equation

$$\begin{Bmatrix} v'_1 \\ v'_2 \\ \vdots \\ v'_n \end{Bmatrix} = \begin{vmatrix} \mu_{11} & \mu_{12} & \dots & \mu_{1j} \\ \mu_{21} & \mu_{22} & \dots & \mu_{2j} \\ \vdots & \vdots & \dots & \vdots \\ \mu_{n1} & \mu_{n2} & \dots & \mu_{nj} \end{vmatrix} \begin{Bmatrix} \beta_{11} \\ \beta_{12} \\ \vdots \\ \beta_{1j} \end{Bmatrix} \quad (13a)$$

or

$$\{v'_n\} = \|\mu_{nj}\| \{\beta_{1j}\} \quad (13b)$$

Premultiplication of both sides of equation (13b) by the matrix of the bridge responses transposed, gives the least-squares normal equation

$$\left[\left\| \mu_{nj} \right\| \right]^T \left\{ v'_n \right\} = \left[\left\| \mu_{nj} \right\| \left\| \mu_{nj} \right\| \right] \left\{ \beta_{1j} \right\} \quad (14)$$

and the values of the load coefficients $\left\{ \beta_{1j} \right\}$ are determined by solution of the j simultaneous equations, or

$$\left\{ \beta_{1j} \right\} = \left[\left\| \mu_{nj} \right\| \left\| \mu_{nj} \right\| \right]^{-1} \left\| \mu_{nj} \right\|^T \left\{ v'_n \right\} \quad (15)$$

When the n loads with shear values v'_n are applied at the n loading points, n values of bending moment and torque are fixed (eq. (2)) and thus the procedure outlined in connection with equations (11) to (15) can also be used to determine the values of $\left\{ \beta_{2j} \right\}$ and $\left\{ \beta_{3j} \right\}$, equation (9), which are needed to evaluate moment and torque.

The necessary condition for the existence of the least-squares solution (15) to equation (14), that the determinant of the matrix of the normal equations is greater than zero, or

$$\left| \left[\left\| \mu_{nj} \right\| \left\| \mu_{nj} \right\| \right] \right| > 0 \quad (16)$$

requires that bridges with similar response characteristics should not be used together.

Selection of Bridges

As pointed out in connection with equations (5) the number of bridges required for a given load equation depends upon the response characteristics of the bridges. Experience has shown that, when shear bridges are placed at a given station on the webs of all spars, bending-moment bridges on the flanges or skin and torque bridges in the torque boxes, enough bridges will be available to develop an equation for shear, or moment, or torque. Usually more than enough bridges are available.

If the j in equation (9) is taken as all of the available bridges, then the particular form the equation should take for a particular structure, that is which of the values of β are zero, depends upon the nature of the structure. Often the form can be determined by analogy with other structures, but some bridges may have such similar characteristics that the output of one is a linear multiple of the output of another, (redundant) or some may be irrelevant ($\beta \approx 0$). Redundancy can sometimes be recognized from examination of the influence-coefficient plots. Irrelevancy is not always so easily determined and an advantage of least-squares solution for the load coefficients lies in the availability of standard statistical methods for determining the reliability and relevancy of any equation. Several checks may be employed. By referring to equation (10) for shear, one check is to substitute the n sets of measured values of bridge response μ_{nj} into the load equation and compare the n calculated values of shear with the n applied values. Defining a residual ϵ as the difference between calculated and applied values, or

$$\{\epsilon_V\} = \{V\} - \{V'\} \quad (17)$$

gives the probable error of estimate of shear values obtained from equation (10) as

$$PE(V) = 0.6745 \sqrt{\frac{\sum \epsilon_V^2}{n - q}} \quad (18)$$

where

n number of loads applied

q number of terms in calibration equation

$\sum \epsilon_V^2$ sum of squares of the residuals which may be calculated from the relationship

$$\sum \epsilon_V^2 = \sum (v'_n)^2 - [\beta_{1j}] \left\{ \|\mu_{nj}\| \right\}^T \{v'_n\} \quad (19)$$

where the column matrix on the right has already been calculated in connection with the solution of equation (15)

The probable error (ref. 10, sections 22.15 and 22.31) in any of the calibration coefficients is obtained from the probable error of estimate for the equation and from the terms on the principal diagonal of the matrix

$$\begin{bmatrix} m_{11} & m_{12} & \dots & m_{1j} \\ m_{21} & m_{22} & \dots & m_{2j} \\ \cdot & \cdot & \dots & \cdot \\ \cdot & \cdot & \dots & \cdot \\ m_{j1} & m_{j2} & \dots & m_{jj} \end{bmatrix} = \left[\left\| \left\| \mu_{nj} \right\| \right\|^T \left\| \left\| \mu_{nj} \right\| \right\| \right]^{-1} \tag{20}$$

where the matrix on the right also appears in the solution of the least-squares normal equation (15). The relation for the probable errors of $\beta_{11}, \beta_{12}, \dots, \beta_{1j}$ is

$$\left\{ \begin{array}{c} PE(\beta_{11}) \\ PE(\beta_{12}) \\ \cdot \\ \cdot \\ PE(\beta_{1j}) \end{array} \right\} = PE(V) \left\{ \begin{array}{c} \sqrt{m_{11}} \\ \sqrt{m_{22}} \\ \cdot \\ \cdot \\ \sqrt{m_{jj}} \end{array} \right\} \tag{21}$$

and similar relationships apply to the probable errors in the load coefficients in equations for bending moment and torque. With the coefficients and their probable errors computed, it is possible to check the calibration equation for inclusion of irrelevant bridges and redundancy. The load coefficient β of an irrelevant bridge is ordinarily small in comparison with its probable error and in comparison with the coefficients of the other bridges. Redundancy is evidenced by large probable errors in all coefficients, generally as a result of large values of $m_{11} \dots m_{jj}$ rather than of the probable error of estimate. Improved results can often be obtained by dropping one or more redundant bridges and recomputing the β coefficients. For detailed comparisons of a number of load equations involving various selections of the available bridges, an objective test of the significance of any improvement is provided by the F-table, see, for example, reference 11.

Procedures for Bridge Combination

When the values of the load coefficients β in equation (9) have been obtained, they can be used directly with the measured outputs of the individual bridges for the evaluation of flight data. Punched-card methods are particularly convenient for handling the large quantities of numerical work involved if loads are required in time-history form. By electrical combination of the output of several bridges, it is, however, possible to simplify flight recording and to reduce data reduction time.

Full combination procedure. - If the shear expression in equation (9) requires j bridges and the load coefficients $\beta_{11} \dots \beta_{1j}$ have been obtained by least squares, the equation for shear would be

$$V = \beta_{11}\mu_1 + \beta_{12}\mu_2 + \dots + \beta_{1j}\mu_j \quad (22)$$

Factoring out the coefficient with the greatest magnitude, say β_{12} , gives

$$V = \beta_{12} \left(\frac{\beta_{11}}{\beta_{12}} \mu_1 + \mu_2 + \dots + \frac{\beta_{1j}}{\beta_{12}} \mu_j \right) \quad (23)$$

By suitable choice of attenuating resistors, the outputs of bridges 1, 3, 4, . . . j can be added to the output of bridge 2 to produce a new combined bridge with an output ρ_V which is proportional to the sum $\frac{\beta_{11}}{\beta_{12}} \mu_1 + \mu_2 + \dots + \frac{\beta_{1j}}{\beta_{12}} \mu_j$. This output is a direct measure of shear alone, or

$$V = \beta' \rho_V \quad (24)$$

A similar procedure can be used to obtain combined channels which provide direct measurements of bending moment or torque. The β' coefficients are obtained by a final calibration, applying loads at various chordwise and spanwise locations as in the preliminary calibration.

An electrical circuit which accomplishes the addition of $\frac{\beta_{11}}{\beta_{12}} \mu_1$ to μ_2 is shown in figure 1(c). The attenuating resistance R_A is related

to the resistance of the individual gages R and to the reciprocal of the combining ratio β_{11}/β_{12} by the equation

$$R_A = \left(\frac{\beta_{12}}{\beta_{11}} - 1 \right) R \quad (25)$$

When the circuit is extended to include more than two bridges, an equation of the form of equation (25) applies to each of the attenuated bridges. Since, however, with direct-current circuits, any given bridge can be used in only one circuit, use of this full combination procedure usually requires multiple installation of the individual strain-gage bridges. If carry-over were present, its use might require that some bridges be installed in sextuplicate. If the number of bridges which could be installed were limited, use of the full combination procedure could restrict the number of loads which could be measured.

Partial combination procedure.- A partial combination procedure can be evolved which strikes a compromise between the data reduction time of the basic procedure (eq. (9)) and the bridge installation requirements of the full combination procedure. In this partial combination procedure, data obtained during a preliminary calibration are used to combine bridges with the same primary sensitivity, that is, the shear sensitive bridges on one side of the structure are combined into a single channel, the moment sensitive bridges on one side into a single channel, and torque sensitive bridges into a single channel. The structure is then recalibrated to determine the final calibration coefficients. The details of the procedure as given below are for a three-spar structure subject to carry-over effects. The procedure can be extended to other structures, or simplified for structures without carry-over.

The bridge installation for the structure chosen to illustrate the procedure is assumed to consist of three sets of shear, moment and torque sensitive bridges on each side (a total of 18 bridges), which by the basic calibration procedure might require the solution of six sets of equations involving as many as eighteen unknowns. Instead a procedure is adopted which involves the solution of six sets of least-squares equations based on certain simplified load equations, containing at most seven coefficients. For example, for left-side shear the equation involves three shear bridges with outputs μ_1 , μ_2 , and μ_3 , the left-side moment, and the three loads applied on the right, or

$$V_L = \beta_{11}\mu_1 + \beta_{12}\mu_2 + \beta_{13}\mu_3 + \beta_{14}M_L + \beta_{15}V_R + \beta_{16}M_R + \beta_{17}T_R \quad (26)$$

By electrical combination of bridges with response μ_1 , μ_2 , and μ_3 a combined channel is obtained with an output primarily sensitive to shear, secondarily responsive to M_L , V_R , M_R , and T_R , and which by the least-squares process has minimized the effects of chordwise position of load on the left side (T_L) and any other terms of the type $Vx^r y^s$.

In matrix notation the β coefficients are computed by a least-squares procedure starting with equation (26) or,

$$V_L = \begin{bmatrix} \mu_1 & \mu_2 & \mu_3 & M_L & V_R & M_R & T_R \end{bmatrix} \begin{Bmatrix} \beta_{11} \\ \beta_{12} \\ \beta_{13} \\ \beta_{14} \\ \beta_{15} \\ \beta_{16} \\ \beta_{17} \end{Bmatrix} \quad (27)$$

The preliminary calibration data for the n values of applied shears and moments and corresponding bridge responses are

$$\begin{Bmatrix} V'_L{}_1 \\ V'_L{}_2 \\ \vdots \\ V'_L{}_n \end{Bmatrix} = \begin{bmatrix} \mu_{11} & \mu_{12} & \mu_{13} & M'_L{}_1 & V'_R{}_1 & M'_R{}_1 & T'_R{}_1 \\ \mu_{21} & \mu_{22} & \mu_{23} & M'_L{}_2 & V'_R{}_2 & M'_R{}_2 & T'_R{}_2 \\ \vdots & \vdots & \vdots & \vdots & \vdots & \vdots & \vdots \\ \mu_{n1} & \mu_{n2} & \mu_{n3} & M'_L{}_n & V'_R{}_n & M'_R{}_n & T'_R{}_n \end{bmatrix} \begin{Bmatrix} \beta_{11} \\ \beta_{12} \\ \beta_{13} \\ \beta_{14} \\ \beta_{15} \\ \beta_{16} \\ \beta_{17} \end{Bmatrix} \quad (28a)$$

or

$$\{V'_L\} = \{R\} \{\beta\} \quad (28b)$$

The least-squares normal equations are

$$\left\{ \left\| R \right\|^T \left\{ V_L \right\} \right\} = \left[\left\| R \right\|^T \left\| R \right\| \right] \left\{ \beta \right\} \tag{29}$$

Therefore

$$\left\{ \beta \right\} = \left[\left\| R \right\|^T \left\| R \right\| \right]^{-1} \left\{ \left\| R \right\|^T \left\{ V_L \right\} \right\} \tag{30}$$

The β coefficients for the preliminary equations for M_L , T_L , V_R , M_R , and T_R are obtained in a similar manner from simplified load equations similar to equation (26) and which may be summarized along with equation (28) in matrix form as

$$\begin{bmatrix} \underline{V_L} & - & - & - & - & - \\ - & \underline{M_L} & - & - & - & - \\ - & - & \underline{T_L} & - & - & - \\ - & - & - & \underline{V_R} & - & - \\ - & - & - & - & \underline{M_R} & - \\ - & - & - & - & - & \underline{T_R} \end{bmatrix} = \begin{bmatrix} \left[\begin{array}{ccc|cccc} \mu_1 & \mu_2 & \mu_3 & V_L & M_L & V_R & M_R & T_R \end{array} \right] & \left[\begin{array}{cccccc} \beta_{11} & \beta_{21} & \beta_{31} & \beta_{41} & \beta_{51} & \beta_{61} \end{array} \right] \\ \left[\begin{array}{ccc|cccc} \mu_4 & \mu_5 & \mu_6 & M_L & V_L & V_R & M_R & T_R \end{array} \right] & \left[\begin{array}{cccccc} \beta_{12} & \beta_{22} & \beta_{32} & \beta_{42} & \beta_{52} & \beta_{62} \end{array} \right] \\ \left[\begin{array}{ccc|cccc} \mu_7 & \mu_8 & \mu_9 & T_L & M_L & V_R & M_R & T_R \end{array} \right] & \left[\begin{array}{cccccc} \beta_{13} & \beta_{23} & \beta_{33} & \beta_{43} & \beta_{53} & \beta_{63} \end{array} \right] \\ \left[\begin{array}{ccc|cccc} \mu_{10} & \mu_{11} & \mu_{12} & V_R & M_R & V_L & M_L & T_L \end{array} \right] & \left[\begin{array}{cccccc} \beta_{14} & \beta_{24} & \beta_{34} & \beta_{44} & \beta_{54} & \beta_{64} \end{array} \right] \\ \left[\begin{array}{ccc|cccc} \mu_{13} & \mu_{14} & \mu_{15} & M_R & V_R & V_L & M_L & T_L \end{array} \right] & \left[\begin{array}{cccccc} \beta_{15} & \beta_{25} & \beta_{35} & \beta_{45} & \beta_{55} & \beta_{65} \end{array} \right] \\ \left[\begin{array}{ccc|cccc} \mu_{16} & \mu_{17} & \mu_{18} & T_R & M_R & V_L & M_L & T_L \end{array} \right] & \left[\begin{array}{cccccc} \beta_{16} & \beta_{26} & \beta_{36} & \beta_{46} & \beta_{56} & \beta_{66} \end{array} \right] \\ & & & & & & & \left[\begin{array}{cccccc} \beta_{17} & \beta_{27} & \beta_{37} & \beta_{47} & \beta_{57} & \beta_{67} \end{array} \right] \end{bmatrix} \tag{31}$$

where the terms on the principal diagonal of the left side are the only ones of interest.

The known load coefficients β_{11} , β_{12} , β_{13} , . . . β_{61} , β_{62} , β_{63} in the upper portion of the β -matrix (eq. (31)) are used to calculate the attenuation required for electrical combination. For example, the attenuation factors for the shear sensitive combined bridge on the left side would be obtained from the equation

$$\rho_{V_L} = \left(\frac{\beta_{11}}{\beta_{1k}} \mu_1 + \frac{\beta_{12}}{\beta_{1k}} \mu_2 + \frac{\beta_{13}}{\beta_{1k}} \mu_3 \right) \tag{32}$$

where β_{lk} denotes the coefficient β_{11} , β_{12} , or β_{13} with the largest magnitude. The six combined bridges with outputs ρ_{V_L} , ρ_{M_L} , ρ_{T_L} , ρ_{V_R} , ρ_{M_R} , and ρ_{T_R} are then recalibrated by applying a set of calibrate loads (not necessarily the same as those used in the preliminary calibration) to the structure. This final calibration should include both symmetrical and unsymmetrical loading conditions. The final equations for use in evaluation of the flight data are of the form

$$\begin{Bmatrix} V_L \\ M_L \\ T_L \\ V_R \\ M_R \\ T_R \end{Bmatrix} = \begin{bmatrix} \beta'_{11} & \beta'_{12} & \beta'_{13} & \beta'_{14} & \beta'_{15} & \beta'_{16} \\ \beta'_{21} & \beta'_{22} & \beta'_{23} & \beta'_{24} & \beta'_{25} & \beta'_{26} \\ \beta'_{31} & \beta'_{32} & \beta'_{33} & \beta'_{34} & \beta'_{35} & \beta'_{36} \\ \beta'_{41} & \beta'_{42} & \beta'_{43} & \beta'_{44} & \beta'_{45} & \beta'_{46} \\ \beta'_{51} & \beta'_{52} & \beta'_{53} & \beta'_{54} & \beta'_{55} & \beta'_{56} \\ \beta'_{61} & \beta'_{62} & \beta'_{63} & \beta'_{64} & \beta'_{65} & \beta'_{66} \end{bmatrix} \begin{Bmatrix} \rho_{V_L} \\ \rho_{M_L} \\ \rho_{T_L} \\ \rho_{V_R} \\ \rho_{M_R} \\ \rho_{T_R} \end{Bmatrix} \quad (33)$$

where the β' coefficients are evaluated by least squares.

APPLICATION OF PROCEDURES

To illustrate the application of the calibration procedures just outlined, the calibration of two representative structures is described in detail. The calibration of these structures presented most of the problems that have arisen in the course of the calibration of a great many structures in the Langley aircraft loads calibration laboratory of the Flight Research Division. In addition they also illustrate the use of the partial and full combination procedures. Structure A is a three-spar unswept horizontal stabilizer and elevator assembly with aspect ratio 6.7, taper ratio 0.29, and 12° dihedral. Structure B is a two-spar horizontal stabilizer with the quarter-chord line swept 35.6° , aspect ratio 4.65, taper ratio 0.45, and 10° dihedral.

The strain-gage locations for structure A are shown in figure 2. Shear and bending-moment bridges of the type shown in figure 1(a) were installed on all three spars at stations parallel to the center line. The strain-gage locations for structure B are shown in figure 3. Shear and bending-moment bridges of the type shown in figure 1(a) were installed

on both spars at station 1 (parallel to the center line) and at station 2 (perpendicular to the sweep axis). In addition, four torque bridges were installed on the skin between the spars at a station perpendicular to the sweep axis, on the left side. The leads from each strain-gage bridge were routed into individual balance circuits. Each circuit, figure 1(b), contained a balance potentiometer R_P and a calibrate resistor R_C . When combined bridges were used, the attenuating resistors were incorporated in the manner indicated in figure 1(c). Changes in current for either individual or combined bridges associated with strain changes in the structure under the application of calibrate loads were recorded by means of a spotlight galvanometer. Bridge sensitivity was made independent of voltage changes by shunting the known calibrate resistor R_C across one arm of either single or combined bridges and measuring the resultant galvanometer deflection δ_{cal} . The calibrate loads applied to each structure whether they were point loads or distributed check loads, were applied in five equal increments and removed in the same increments. Values of the galvanometer deflection δ were recorded for each load increment. A straight line of the form

$$\delta = k_1 + k_2 V \quad (34)$$

was fitted to the 11 data points by means of least squares, and the deflection used for the loading was the value given by the product of the least-squares slope k_2 and the calibrate load, or

$$\delta_{max} = k_2 \times \text{calibrate load} \quad (35)$$

The value of μ (or ρ) corresponding to the calibrate load was then taken as

$$\mu = \frac{\delta_{max}}{\delta_{cal}} \quad (36)$$

An attempt was made to minimize any possible effects of elastic lag by running through several cycles of load before taking data, and by taking as a reference condition not the no-load condition but a datum determined by a preload.

Structure A

The application of calibration procedures for obtaining shear and bending moment on a structure where large carry-over effects were present

is illustrated by structure A where the partial gage combination procedure was used in order to measure both symmetrical and unsymmetrical tail loads in flight with as few recording channels and as few strain gages as possible. The relationship between individual strain-gage response and applied loads for the structure was obtained by applying point loads at three spanwise and three chordwise positions per side for both the preliminary and final calibrations. The chord and semi-span locations of applied loads are shown in figure 4 and the values of shear and bending moment are given in table I. Point loads were applied to the left side alone, the right side alone, and to both sides simultaneously.

Preliminary calibration.- The nondimensional bridge response values μ for each of the 12 bridges for each of the 27 loads are given in table I, and the influence-coefficient plots μ/V are presented in figures 5 to 8. To illustrate trends, curves have been faired through the data points. The equations for determining the load coefficients for electrical combination were based on equation (31) without torque measurement and some simplifications suggested by examination of the influence-coefficient plots (figs. 5 to 8). The simplified equations are summarized in matrix form as

$$\begin{bmatrix} V_L & - & - & - & - & - \\ - & M_L & - & - & - & - \\ - & - & - & - & - & - \\ - & - & - & V_R & - & - \\ - & - & - & - & M_R & - \\ - & - & - & - & - & - \\ - & - & - & - & - & - \end{bmatrix} = \begin{bmatrix} \mu_{V_{LF}} & \mu_{V_{LM}} & \mu_{V_{LR}} & M_L & - & M_R & - \\ \mu_{M_{LF}} & \mu_{M_{LM}} & \mu_{M_{LR}} & - & - & M_R & - \\ - & - & - & - & - & - & - \\ \mu_{V_{RF}} & \mu_{V_{RM}} & \mu_{V_{RR}} & M_R & - & M_L & - \\ \mu_{M_{RF}} & \mu_{M_{RM}} & \mu_{M_{RR}} & - & - & M_L & - \\ - & - & - & - & - & - & - \\ - & - & - & - & - & - & - \end{bmatrix} \begin{bmatrix} a_{11} & a_{21} & - & a_{41} & a_{51} & - \\ a_{12} & a_{22} & - & a_{42} & a_{52} & - \\ a_{13} & a_{23} & - & a_{43} & a_{53} & - \\ - & - & - & - & - & - \\ a_{14} & - & - & a_{44} & - & - \\ - & - & - & - & - & - \\ a_{16} & a_{26} & - & a_{46} & a_{56} & - \\ - & - & - & - & - & - \end{bmatrix} \quad (37)$$

where the subscripts on the strain-gage response μ denote the primary sensitivity and location of the bridge, and the β_{ij} of equation (31) have been replaced for structure A by the symbol a_{ij} . The values determined for a_{11} to a_{56} by least-square procedures are given together with their probable errors in the top half of table II.

By using the procedure of equation (32) and the largest a coefficients given in table II, the strain-gage bridges of equation (37)

were combined electrically to produce four partially combined bridges according to the following equations:

$$\left. \begin{aligned}
 \rho_{V_L} &= \frac{a_{11}}{a_{12}} \mu_{V_{LF}} + \mu_{V_{LM}} + \frac{a_{13}}{a_{12}} \mu_{V_{LR}} \\
 \rho_{M_L} &= \frac{a_{21}}{a_{22}} \mu_{M_{LF}} + \mu_{M_{LM}} + \frac{a_{23}}{a_{22}} \mu_{M_{LR}} \\
 \rho_{V_R} &= \frac{a_{41}}{a_{43}} \mu_{V_{RF}} + \frac{a_{42}}{a_{43}} \mu_{V_{RM}} + \mu_{V_{RR}} \\
 \rho_{M_R} &= \frac{a_{51}}{a_{52}} \mu_{M_{RF}} + \mu_{M_{RM}} + \frac{a_{53}}{a_{52}} \mu_{M_{RR}}
 \end{aligned} \right\} \quad (38)$$

Final calibration. - The structure was loaded again with the same loads as in the preliminary calibration. Influence-coefficient plots for ρ_{V_L} , ρ_{M_L} , ρ_{V_R} , and ρ_{M_R} (fig. (9)) show the response of the combined bridges to the loads applied in the final calibration. The final shear and bending-moment equations, which were similar to equation (33), were

$$\left\{ \begin{array}{c} V_L \\ M_L \\ V_R \\ M_R \end{array} \right\} = \begin{bmatrix} a'_{11} & a'_{12} & a'_{13} & a'_{14} \\ a'_{21} & a'_{22} & a'_{23} & a'_{24} \\ a'_{31} & a'_{32} & a'_{33} & a'_{34} \\ a'_{41} & a'_{42} & a'_{43} & a'_{44} \end{bmatrix} \left\{ \begin{array}{c} \rho_{V_L} \\ \rho_{M_L} \\ \rho_{V_R} \\ \rho_{M_R} \end{array} \right\} \quad (39)$$

The final calibration coefficients a'_{11} to a'_{44} are given in table II. Also given in table II are the probable errors of estimate obtained by the use of equation (18) and the probable errors in the coefficients obtained from equation (21). Zeroes in table II indicate that the corresponding bridges were found to be irrelevant.

As a check on the applicability of equations obtained by the point load calibration to the determination of distributed loads as encountered

in flight, the distributed load A shown in figure 10 was applied to the structure. For this loading the gage response, the applied and calculated values of shear and bending moment, the differences, and the percentage differences are given in table III. Sample calculations for the preliminary and final left shear load coefficients for structure A together with the probable errors are presented in table IV.

Structure B

The application of calibration procedures for obtaining shear, bending moment, and torque on a swept structure is illustrated by structure B for which a form of the full combination procedure was used. The data for structure B were obtained as part of a general investigation of calibration methods applied to swept structures. For this reason, although structure B is a horizontal stabilizer and carry-over effects were present, these effects were ignored in the preliminary calibration, and the data treated as it would be for a wing where carry-over effects are ordinarily not observed. For the final calibration, however, carry-over effects were included.

Preliminary calibration.- The preliminary calibrated loads were applied on the left side alone and on the right side alone. The chordwise and semispan locations of applied loads are shown in figure 11 and the associated values of shear, moment, and torque are given in table V. For the 16 bridges shown in figure 3, the bridge response coefficients μ corresponding to each point load are given in table V and the corresponding influence-coefficient values in figures 12 to 16. In figure 17, the influence-coefficient data for the left shear and the left moment bridges at gage station 2 have also been plotted against the distance along the sweep line, measured from the intersection of the sweep axis and the center line.

Of the many equations which might have been used to relate load to the outputs of the various bridges located on either the left or right sides, only a limited number were investigated. The limitation was guided by the nature of the influence-coefficient plots. The similarity of the response of each of the four torque bridges (fig. 16) suggests that redundancies will be introduced if more than one torque bridge is included in any equation. The similarity of the response of both front and rear spar moment bridges (figs. 14 and 15) and the comparative absence of both shear effects and nonlinearities in the moment curves imply that little would be gained by using two moment bridges; the rear spar bridges actually used had the highest moment sensitivity as shown by the greater slope of the influence-coefficient plots. These considerations suggested that the equations for the left side be limited to two shear bridges, a bending-moment bridge, and one of the four torque bridges. Equations for the right side were limited to two shear

bridges and a moment bridge. Although only one torque bridge was to be used in the equations for the left side, a check was made to determine which of the torque bridges gave the best results. For the shear, bending moment, and torque at station 1 and shear and bending moment at station 2, this check involved a least-squares calculation of the coefficients of four different equations each involving a different torque bridge (20 solutions in all). These equations can be represented by the general form

$$\left\{ L_p \right\} = \begin{bmatrix} b_{p1} & b_{p2} & b_{p3} & b_{p4} \\ b_{p1} & b_{p2} & b_{p3} & b_{p4} \\ b_{p1} & b_{p2} & b_{p3} & b_{p4} \\ b_{p1} & b_{p2} & b_{p3} & b_{p4} \end{bmatrix} \begin{Bmatrix} \mu_{V_{LF1}} \\ \mu_{V_{LF2}} \\ \mu_{V_{LR}} \\ \mu_{M_{LR}} \end{Bmatrix} + \begin{bmatrix} b_{p5} & 0 & 0 & 0 \\ 0 & b_{p6} & 0 & 0 \\ 0 & 0 & b_{p7} & 0 \\ 0 & 0 & 0 & b_{p8} \end{bmatrix} \begin{Bmatrix} \mu_{T_{FT}} \\ \mu_{T_{FB}} \\ \mu_{T_{RT}} \\ \mu_{T_{RB}} \end{Bmatrix} \quad (40)$$

where L_p is a general load term and values of p from 1 to 5 correspond respectively to V_{L1} , M_{L1} , T_{L1} , V_{L2} , and M_{L2} . Although both b_{p1} and b_{p2} are shown in equation (40), only the appropriate value is used for calculations at station 1 or station 2. The values of the coefficients b_{11} , . . . b_{58} are given in table VI along with the probable errors and the probable error of estimate of each of the equations. The coefficients were calculated by solution of the least-squares normal equations of the form of equation (15) obtained from the calibration data of table V.

The probable errors of the coefficients were calculated by equations of the form of equation (21) and the probable errors of estimate by means of equations of the form of equation (18).

The bridges selected for combination were those with the smallest value of probable error and are indicated by asterisks in table VI. The equations corresponding to the selected bridge combinations were

$$\begin{Bmatrix} V_{L1} \\ M_{L1} \\ T_{L1} \\ V_{L2} \\ M_{L2} \end{Bmatrix} = \begin{bmatrix} b_{11} & 0 & b_{13} & b_{14} \\ b_{21} & 0 & b_{23} & b_{24} \\ b_{31} & 0 & b_{33} & b_{34} \\ 0 & b_{42} & b_{43} & b_{44} \\ 0 & b_{52} & b_{53} & b_{54} \end{bmatrix} \begin{Bmatrix} \mu_{V_{LF1}} \\ \mu_{V_{LF2}} \\ \mu_{V_{LR}} \\ \mu_{M_{LR}} \end{Bmatrix} + \begin{bmatrix} 0 & 0 & b_{17} \\ 0 & 0 & b_{27} \\ b_{35} & 0 & 0 \\ 0 & 0 & b_{47} \\ 0 & b_{56} & 0 \end{bmatrix} \begin{Bmatrix} \mu_{T_{FT}} \\ \mu_{T_{FB}} \\ \mu_{T_{RT}} \end{Bmatrix} \quad (41)$$

For the right side where torque bridges were not installed, the equations for shear, bending moment, and torque at station 1 and shear and bending moment at station 2 were

$$\begin{Bmatrix} V_{R1} \\ M_{R1} \\ T_{R1} \\ V_{R2} \\ M_{R2} \end{Bmatrix} = \begin{bmatrix} b_{11} & 0 & b_{13} & b_{14} \\ b_{21} & 0 & b_{23} & b_{24} \\ b_{31} & 0 & b_{33} & b_{34} \\ 0 & b_{42} & b_{43} & b_{44} \\ 0 & b_{52} & b_{53} & b_{54} \end{bmatrix} \begin{Bmatrix} \mu_{V_{RF1}} \\ \mu_{V_{RF2}} \\ \mu_{V_{RR}} \\ \mu_{M_{RR}} \end{Bmatrix} \quad (42)$$

Values of the load coefficients b_{11}, \dots, b_{54} (eq. (42)) are given in table VII together with their probable errors and the probable errors of estimate of the equations, all obtained in the same manner as with table VI. Also shown in table VII are additional equations for M_{R1} and V_{R2} , indicated by asterisks, which were calculated when it was found that the rear shear bridge in the equation for M_{R1} and the rear moment bridge in the equation V_{R2} were irrelevant. The coefficients of the bridges which were omitted were small with respect to their probable errors, and with respect to the terms which were retained.

Based on the preliminary calibration coefficients given in tables VI and VII, the strain-gage bridges of equations (41) and (42) were combined electrically to produce combined bridges, according to the following equations:

For the left side:

$$\left. \begin{aligned} \rho_{V_{L1}} &= \mu_{V_{LF1}} + \frac{b_{13}}{b_{11}} \mu_{V_{LR}} + \frac{b_{14}}{b_{11}} \mu_{M_{LR}} + \frac{b_{17}}{b_{11}} \mu_{T_{RT}} \\ \rho_{M_{L1}} &= \frac{b_{21}}{b_{24}} \mu_{V_{LF1}} + \frac{b_{23}}{b_{24}} \mu_{V_{LR}} + \mu_{M_{LR}} + \frac{b_{27}}{b_{24}} \mu_{T_{RT}} \\ \rho_{T_{L1}} &= \frac{b_{31}}{b_{34}} \mu_{V_{LF1}} + \frac{b_{33}}{b_{34}} \mu_{V_{LR}} + \mu_{M_{LR}} + \frac{b_{35}}{b_{34}} \mu_{T_{FT}} \\ \rho_{V_{L2}} &= \frac{b_{42}}{b_{43}} \mu_{V_{LF2}} + \mu_{V_{LR}} + \frac{b_{44}}{b_{43}} \mu_{M_{LR}} + \frac{b_{47}}{b_{43}} \mu_{T_{RT}} \\ \rho_{M_{L2}} &= \frac{b_{52}}{b_{54}} \mu_{V_{LF2}} + \frac{b_{53}}{b_{54}} \mu_{V_{LR}} + \mu_{M_{LR}} + \frac{b_{56}}{b_{54}} \mu_{T_{FB}} \end{aligned} \right\} \quad (43)$$

and for the right side,

$$\left. \begin{aligned}
 \rho_{V_{R_1}} &= \mu_{V_{RF_1}} + \frac{b_{13}}{b_{11}} \mu_{V_{RR}} + \frac{b_{14}}{b_{11}} \mu_{M_{RR}} \\
 \rho_{M_{R_1}} &= \frac{b_{21}}{b_{24}} \mu_{V_{RF_1}} + \mu_{M_{RR}} \\
 \rho_{T_{R_1}} &= \frac{b_{31}}{b_{34}} \mu_{V_{RF_1}} + \frac{b_{33}}{b_{34}} \mu_{V_{RR}} + \mu_{M_{RR}} \\
 \rho_{V_{R_2}} &= \mu_{V_{RF_2}} + \frac{b_{43}}{b_{42}} \mu_{V_{RR}} \\
 \rho_{M_{R_2}} &= \frac{b_{52}}{b_{54}} \mu_{V_{RF_2}} + \frac{b_{53}}{b_{54}} \mu_{V_{RR}} + \mu_{M_{RR}}
 \end{aligned} \right\} \quad (44)$$

Final calibration.- The relationship between applied load and the response of bridges combined according to equations (43) and (44) was then obtained by applying 15 point loads per side. In this final calibration, symmetrical point loads were applied in addition to left and right unsymmetrical loads. The chordwise and spanwise locations of applied load for the final calibration are shown in figure 11. Since a given bridge was required in more than one equation of equations (43) and (44), a switching arrangement was employed in the calibration which automatically set up each combined bridge in sequence during the application of each point load. The values of ρ corresponding to each point load are tabulated in table VIII. Influence-coefficient plots for the combined bridges are given in figures 18 to 20 for the unsymmetrical loadings for both swept and unswept coordinate axes.

Had carry-over effects not been present, the data of table VIII would have been used simply to obtain the final load coefficient b' and this procedure could ordinarily be used with wings, and for strain-gage stations located other than at the root. In order to provide a calibration which would permit evaluation of loads on both sides of the horizontal tail allowing for the carry-over effects actually present, the data of table VIII were used to compute the final calibration

coefficients to be used in final equations involving bridges on both sides of the structure. In general, these equations would have the form

$$\begin{Bmatrix} V_{L1} \\ M_{L1} \\ T_{L1} \\ V_{L2} \\ M_{L2} \\ V_{R1} \\ M_{R1} \\ T_{R1} \\ V_{R2} \\ M_{R2} \end{Bmatrix} = \begin{bmatrix} b'_{11} & 0 & 0 & 0 & 0 & b'_{16} & b'_{17} & b'_{18} & 0 & 0 \\ 0 & b'_{22} & 0 & 0 & 0 & b'_{26} & b'_{27} & b'_{28} & 0 & 0 \\ 0 & 0 & b'_{33} & 0 & 0 & b'_{36} & b'_{37} & b'_{38} & 0 & 0 \\ 0 & 0 & 0 & b'_{44} & 0 & b'_{46} & b'_{47} & b'_{48} & 0 & 0 \\ 0 & 0 & 0 & 0 & b'_{55} & b'_{56} & b'_{57} & b'_{58} & 0 & 0 \\ b'_{61} & b'_{62} & b'_{63} & 0 & 0 & b'_{66} & 0 & 0 & 0 & 0 \\ b'_{71} & b'_{72} & b'_{73} & 0 & 0 & 0 & b'_{77} & 0 & 0 & 0 \\ b'_{81} & b'_{82} & b'_{83} & 0 & 0 & 0 & 0 & b'_{88} & 0 & 0 \\ b'_{91} & b'_{92} & b'_{93} & 0 & 0 & 0 & 0 & 0 & b'_{99} & 0 \\ b'_{10,1} & b'_{10,2} & b'_{10,3} & 0 & 0 & 0 & 0 & 0 & 0 & b'_{10,10} \end{bmatrix} \begin{Bmatrix} \rho_{V_{L1}} \\ \rho_{M_{L1}} \\ \rho_{T_{L1}} \\ \rho_{V_{L2}} \\ \rho_{M_{L2}} \\ \rho_{V_{R1}} \\ \rho_{M_{R1}} \\ \rho_{T_{R1}} \\ \rho_{V_{R2}} \\ \rho_{M_{R2}} \end{Bmatrix} \quad (45)$$

but all of the carry-over terms may not be required in any particular case. The values of the coefficients actually needed in these equations are listed in table IX together with the values of the probable error of estimate of each of the 10 equations.

As a check on these equations, three distributed loads B_1 , B_2 , and B_3 shown in figure 21 were applied to the structure. For these loadings, the response of each of the 10 combined bridges, the applied and calculated values of shear, bending moment, and torque, the differences and percentage differences are given in table X.

DISCUSSION

Structure A

The influence-coefficient plots, figures 5 to 8, for the point loads applied during the preliminary calibration of test structure A show that the response of the individual bridges to shear, moment, and torque is not as defined by equation (3), but includes some of the additional terms shown in equation (4). The torque effect is small in the midspar shear bridges (figs. 5(b) and 6(b)) and absent in the midspar moment bridges (figs. 7(b) and 8(b)). With the exception of the left midspar moment bridge (fig. 8(b)) the moment bridges are comparatively free of the effects of nonlinearity, as shown by the straightness of the lines for the loading on each spar. In general, the response of each bridge to

carry-over is similar to the character of the response of the bridge to loads on the same side. The principal carry-over effect is one of bending moment.

Comparison of the probable errors of estimate of the preliminary partial combination equations given in table II with the average applied loads shows that the simplified equation (37) is adequate for eliminating the effects of torque and the other terms in equation (4) responsible for curvature in the influence coefficient plots. Although equations similar to equation (31) were not tested, it appears doubtful that their use would have given significantly better preliminary load coefficients for determining the combining ratios.

The responses ρ_{V_L} , ρ_{M_L} , ρ_{V_R} , and ρ_{M_R} of the four combined bridges based on the data of table II and equation (38) and shown in figure 9 in influence-coefficient form indicate that the combined bridges are essentially free of the effects of chord position of load. They are affected to some extent by moment on the opposite side, since in writing equations of the form of equation (37) this effect is not eliminated until the final calibration. The final equations for evaluating V_L , M_L , V_R , and M_R used for evaluating these loads in flight and given in the lower half of table II indicate probable errors of estimate and probable errors in the coefficients of the same order of magnitude as the preliminary equations. The probable errors of estimate are roughly 1 percent of the average applied loads. The comparison shown in table III of the applied check load A_1 with the loads given by the final equations shows that the differences are less than would be expected from the size of the probable errors in the coefficients of the final equations. In general, these errors are of the same order of magnitude as the experimental errors.

Structure B

The influence-coefficient plots for the shear, moment, and torque bridges of structure B, figures 12 to 16 show marked curvatures of the sort which may be ascribed to the presence of the higher-order terms of equation (4). When values of the influence coefficients for bridges at station 2 (fig. 17) are plotted against distance along the sweep axis, the plots show the same curvatures as are shown in figures 13 and 15, but front- and rear-spar bridges reflect more clearly the effects of the chord position of the load relative to the bridge location, as in structure A. Thus measurement of loads on axes related to the sweep axes may be treated in the same way as measurement of loads on an unswept structure. In view of the similarities between the influence-coefficient plots of bridges at station 1 (parallel to the center line) and those of station 2 (perpendicular to the sweep axis), the use of

strain-gage bridges in the root area of a swept structure does not appear to present any problems which are essentially different from the use of bridges in the root area of an unswept structure. The use of such bridges offers the additional advantages of moment and torque axes which correspond to the usual axes for load distribution and airplane stability determinations.

The preliminary combining equations for the left side, equation (41), and the right side, equation (42), differ since more bridges with different characteristics were available on the left side than on the right. Comparison of the values of probable error of estimate for the best preliminary equations, table VI, with the corresponding probable errors of estimate given in table VII shows that load measurements on the left are probably more accurate than those on the right.

As an illustration of the improvement in measurement of shear on the left using the four bridges combined according to equation (41) for V_{L1} , over the results which would be obtained by using say only the front-spar shear bridge at station 1, the application of least squares and the data of table V to an equation of the type $V_{L1} = b\mu_{V_{LF1}}$ shows that

$$V_{L1} = 1071\mu_{V_{LF1}}$$

and the probable error of estimate P.E. (V_{L1}) is 92 pounds. Had this measurement been attempted by using the best combination of both front- and rear-spar shear bridges the equation would have been

$$V_{L1} = 558\mu_{V_{LF1}} \text{ and } 336\mu_{V_{LR}}$$

and the probable error would have been 29 pounds. Addition of the rear-spar moment bridge gives

$$V_{L1} = 608\mu_{V_{LF1}} + 389\mu_{V_{LR}} - 194\mu_{M_{LR}}$$

with a probable error of 13 pounds, while addition of the torque sensitive shear type of bridge in the rear top torque box gives the equation (from table VI)

$$V_{L1} = 545\mu_{V_{LF1}} + 440\mu_{V_{LR}} - 220\mu_{M_{LR}} + 105\mu_{T_{RT}}$$

with a probable error of estimate of 9 pounds. The improvement in each equation in turn as measured by the probable error of estimate is statistically significant.

The outputs of the combined bridges, with outputs given by equations (43) and (44) should have been pure shear, moment, or torque insofar as the asymmetrical loadings are concerned. As shown by the spanwise or chordwise variations of the values of influence coefficient, figures 18 to 20, the combined shear bridges are very nearly pure shear bridges; for the moment bridges the influence coefficient varies directly with the distance outboard of the gage station, and for the torque bridge, (fig. 20) the influence coefficient varies directly with distance from the torque reference axis. As in the case of the probable errors of estimate, the combined bridges on the left side are generally better than the combined bridges on the right. These plots also indicate a loss of response for the shear bridges at station 2 (fig. 19) when the load is applied on the front spar in the vicinity of the bridge station. A similar loss of response was evident for the front-spar shear bridges at station 2, figures 12(b) and 13(b). This loss in sensitivity appears to be a local effect, associated with the fact that a bridge does not, in general, respond to a load applied inboard of the bridge, and it has only a limited influence on the precision with which shear can be determined.

Examination of the effects of carry over, shown in table VIII and figures 18 and 19 shows that in three out of the ten cases ($\rho_{V_{L_2}}$, $\rho_{T_{L_1}}$, and $\rho_{M_{R_1}}$) bridges combined on the basis of loads applied to the same side had negligible carry-over effects. When final combining equations (45) were developed, application of least-squares principles showed that in these three cases the coefficients for all the bridges on the opposite side could be neglected, as shown by the zeroes in the equations for V_{L_2} , T_{L_1} , and M_{R_1} presented in table IX. In the case of V_{L_2} , and T_{R_1} , the final equations required the inclusion of an additional bridge on the same side.

The final equations shown in table IX have probable errors of estimate of roughly the same order of magnitude as the experimental data. The shear values of the three distributed loads B_1 , B_2 , and B_3 obtained from the final shear equations, are, for station 1 more accurate for the left side than for the right side (see table X.) For station 2, the shear values for the left side are not so accurate as for the right, but are still within the limits that would be estimated from the probable errors of the load coefficients. When the distributed check loads were applied with sand bags to structure B, center-of-pressure locations could not be held to the precise limits possible with the

relatively smaller pads used for applying point loads. A comparison, therefore, of the differences between calculated and applied bending-moment values for the left and right sides is not especially significant. The largest difference in inch-pounds is equivalent to an error in center-of-pressure location for the distributed load of 1.8 inches or 2 percent of the semispan.

Application to Other Structures

Outline of steps in calibration procedure.- Application of the basic load calibration method to wings and vertical tails differs in no essential detail from the general procedures just described for the two horizontal stabilizers. Since the basis of the method is general, the method is applicable to other types of aircraft structures, such as control surfaces or landing gears. No hard and fast rules of procedure can be given which will apply to all cases, since each structure presents individual problems, some of which cannot be recognized until the data of the preliminary calibration are analyzed. Certain steps which are common to all calibrations may be outlined, however, and the first of these is installation of the strain-gage bridges. Shear- or moment-type bridges should be so oriented as to respond primarily to the forces or moments which they are intended to measure. Since it can usually be assumed that such bridges will respond not only to the desired force or moment, but to other forces or moments as well, enough bridges must be installed to permit development of the appropriate equations relating load and bridge response.

The second step in the calibration procedure involves a choice of the calibrate loads. This choice involves a selection of the points of application and the shear values to be applied at these points. For the principal lifting surfaces a minimum would appear to be three chordwise positions at each of three spanwise stations of each panel. The shear values will ordinarily be determined by a safe local stress.

The third step is application of the calibrate loads. These are ordinarily most easily applied with jacks through pads large enough to prevent local buckling. In order to assess any possible effects of elastic lag, application and removal of these loads by increments is recommended. To provide data for evaluating the effects of carry-over the loads should be applied to one side alone, to the other side alone, and to both sides simultaneously, as with structure A.

The fourth step in the calibration procedure involves evaluation of the preliminary calibration data. Influence-coefficient plots provide a useful guide to the characteristics of each bridge, and thus assist in establishing the form of the preliminary calibration equations. A further guide as to the choice of bridges lies in calculation

of the probable error of estimate and the probable errors of the load coefficients of the preliminary equations.

The final step in the calibration procedure depends upon the results of the preliminary calibration, in relation to the electrical recording equipment available and the number of different loads which it is desired to measure in flight. If measurements of shear, bending moment, and torque are desired, and carry-over effects are present such that all bridges are affected by shear, bending moment, and torque of both sides, then full electrical combination appears to be impracticable since all bridges would need to be installed in sextuplicate. On the other hand, these six quantities could all be determined by numerical evaluation of the individually recorded responses of a much smaller number of bridges. An example of a compromise between these two extremes was provided by structure A where a partial combination procedure was used which required only four recording channels for flight measurement and did not require the multiple installation of strain-gage bridges. If a bridge-combination procedure is to be used for flight recording, the structure must be recalibrated in order to determine the final calibration coefficients. A distributed load should also be applied as a check on the final calibration equations. For wing structures where application of distributed loads may not be practicable, check loads may be applied through the jacking points.

Flight load measurements.- A strain-gage installation calibrated according to the methods given in the present paper will measure structural loads relative to some reference condition. The load on the airplane on the ground is the most easily determined reference condition. Provided the landing gear is inboard of the strain-gage station, changes in strain-gage response from the ground to flight at lg are proportional to the aerodynamic load. If the airplane weight is carried at points outboard of the strain-gage station, corrections for the wheel reaction are applied. Corrections must also be applied for any changes in weight distribution outboard of the strain-gage station. Under accelerated flight conditions the loads measured by the strain-gage installation are structural loads and inertia loads must be added in order to obtain aerodynamic load.

Some instrumentation requirements.- Strain-gage installation methods such as those given in references 12 and 13 are satisfactory for loads measurement, provided four active arm bridges with matched individual gages and short interconnecting leads are employed, as illustrated in figure 1. Direct-current systems at present provide the most stable circuit characteristics for measuring bridge output, and thus are being used for flight aerodynamic loads measurements by the NACA.

Because of the possibility of sensitivity changes or of zero drift in the recording apparatus, provision must also be made to account for

such changes. Changes in sensitivity result from changes in supply voltage to the strain-gage bridge and to the recording galvanometer elements; drift results from temperature effects on the galvanometer elements and from temperature effects on the structure. Although drift due to changes in temperature is minimized by the use of four-active-arm bridges, as shown in figure 1, stresses introduced by temperature gradients within the structure are not compensated and a temperature-calibration procedure would be needed if these effects were appreciable. Although sensitivity changes and galvanometer drift are generally small with direct-current strain-gage equipment, in practice it has been desirable to take calibrate signals along with the ground zero records and before each run in flight. A no-voltage galvanometer zero is also recorded on the ground and before each run in flight. With the use of this information, corrections can be applied to the strain-gage-deflection data of each run to refer it to a ground reference condition, which eliminates the necessity for establishing in-flight reference conditions by means of special maneuvers.

CONCLUDING REMARKS

The general principles outlined in the previous sections have been successfully applied to many more structures than have been used as examples in this report. Although the point load method has for some time been the standard calibration procedure at the NACA, the particular methods for reducing the data and of combining gages given in the present report are the result of continual improvements. They are still subject to a certain extent to the judgment and experience of the engineer. Although improvements in detail are still possible, it appears that future work should include the effects of temperature gradients within the structure in anticipation of measuring loads under supersonic-flight conditions where thermal effects may be appreciable.

Langley Aeronautical Laboratory
National Advisory Committee for Aeronautics
Langley Field, Va.

APPENDIX

SIMPLIFIED CALIBRATION PROCEDURES

The fact that the response of several bridges in structures A and B is apparently adequately represented by the simple linear relation

$$\mu_i = \alpha_{i1}V + \alpha_{i2}M + \alpha_{i3}T$$

for certain regions of load application suggests that the calibration procedures outlined in the present report could be considerably simplified. One such simplification could be the arbitrary application of three calibrate loads to a structure with three bridges, and determination of the calibration coefficients by the solution of the three sets of three simultaneous equations.

If small departures from the preceding equation exist, the values of the coefficients obtained depend upon the three points chosen for load application. In addition small errors in measurement greatly influence the values of the coefficients. Unlike results obtained by least squares, the solution of three such simultaneous equations offers no information about the reliability and does not permit assessment of reliability for other loading conditions. Since neither the effect of errors in measurement, nor the existence of small departures from the previous equation can be determined from three applied loads, such a simplified point load calibration is not recommended.

All the disadvantages inherent in simultaneous-equation solution for calibration coefficients are present in a commonly used method of calibration in which a pure shear, a pure torque, and a pure bending moment are applied to a structure and coefficients determined by simultaneous-equation solutions involving the response of three bridges to the three applied pure loads. Conformity to the previous equation cannot be established by the application of only one pure shear, one pure bending moment, and one pure torque but only by the application of loads at many chordwise and spanwise stations. Since the application of many pure loads to a structure is also difficult (requiring special jigs and fittings), it offers no particular advantages as a calibration procedure.

The maximum value of load which can ordinarily be applied to a structure at a given point without risk of local failure is in many instances small as compared with the magnitude of the loads measured in

flight. A method of calibration which permits the use of large distributed loads has also been investigated. This method in certain limited applications would permit the determination of not only the total load, but also the magnitudes of the various components such as the additional and basic air load distributions. The basis of the method lies in the fact that, for a particular distribution of load, the response of a strain-gage bridge will vary linearly with the magnitude of that load. Considering the total load to be made up of several such distributions, some of which will be symmetrical or antisymmetrical zero-lift distributions but all of which will have root-bending-moment values M_1, \dots, M_n , the following equations may be written to express the response of n different bridges to the n loads:

$$\{\mu_i\} = [\alpha_{ij}] \{M_j\} \quad (A1)$$

$$\begin{aligned} i &= 1, 2, 3, \dots, n \\ j &= 1, 2, 3, \dots, n \end{aligned}$$

The coefficients α_{ij} are determined from the strain responses μ_i for loads M_1 to M_n as

$$\alpha_{ij} = \frac{\mu_i}{M_j} \quad (A2)$$

The equations for use in evaluating the load components are then given by

$$\{M_j\} = [\alpha_{ij}]^{-1} \{\mu_i\} \quad (A3)$$

The total moment on the structure is

$$M = \sum M_j \quad (A4)$$

The shear components V_j are

$$V_j = \frac{M_j}{y_j} \quad (A5)$$

and the total shear is

$$V = \sum V_j \quad (A6)$$

The torque components T_j are

$$T_j = k_j M_j \quad (A7)$$

where k_j expresses the exact relationship which exists between the moment and torque for any particular load distribution. The total torque is

$$T = \sum T_j \quad (A8)$$

In practice, if four strain-gage bridges were available, four different load distributions representing the principal components of the load on say a wing panel such as additional, basic, aileron deflection, and damping in roll distributions could be applied in the calibration. The method suffers from the disadvantages inherent in solutions based on simultaneous equations involving an equal number of loads and bridges. If the flight loads were actually a composite of various proportions of the calibrate load distributions, then useful information about distribution could be obtained, but changes in the shape of any one distribution can result in unrealistic values for all the distributions. A comprehensive test of the distributed load calibration method has been made. The data which illustrated the importance of the foregoing shortcomings are not included in the present report, since it is believed that such a method of studying flight loads would be restricted to low-speed tests of rigid structures, and is not sufficiently flexible to give useful information in general flight loads investigations.

REFERENCES

1. Howland, W. L., and Buzzetti, C. J.: Measurements in Flight of Spanwise Wing Loading. Preprint No. 181, Presented at Seventeenth Annual Meeting of Inst. Aero. Sci., Jan. 24-27, 1949.
2. Weiss, David: Flight Load Investigation of Model FG-1 Airplane Empennage — Instrumentation for. Rep. TED No. NAM 2447, pt. I, NAES, Philadelphia Navy Yard, Bur. Aero., May 31, 1944.
3. Morrel, J. S.: Flight Load Investigation of Model FG-1 Airplane Empennage — Calibration Loading and Flight Tests. Rep. TED No. NAM 2447, pt. II, NAES, Philadelphia Navy Yard, Bur. Aero., Aug. 7, 1944.
4. Walter, Maurice A.: Structural Load Measurements on Complex Aircraft Components Using Strain-Gage Summation Circuits. Jour. Aero. Sci., vol. 18, no. 2, Feb. 1951, pp. 101-106.
5. Rogin, L.: Structural Flight Load Measurements — Calibration for — General Theory and Techniques. Rep. No. ASL NAM DE-249.1, NAES, Philadelphia Navy Yard, Bur. Aero., May 22, 1951.
6. Stokke, Allen R., and Aiken, William S., Jr.: Flight Measurement of Buffeting Tail Loads. NACA TN 1719, 1948.
7. Aiken, William S., Jr., and Howard, Donald A.: A Comparison of Wing Loads Measured in Flight on a Fighter-Type Airplane by Strain-Gage and Pressure-Distribution Methods. NACA TN 1967, 1949.
8. Aiken, William S., Jr., and Wiener, Bernard: Time Histories of Horizontal-Tail Loads on a Jet-Powered Bomber in Four Maneuvers. NACA RM L9H16a, 1949.
9. Cooney, T. V.: The Unsymmetrical Load and Bending Moment on the Horizontal Tail of a Jet-Powered Bomber Measured in Sideslipping Flight. NACA RM L51J24, 1952.
10. Kendall, Maurice G.: The Advanced Theory of Statistics. Vol. II, second ed., Charles Griffin and Co., Ltd. (London), 1948.
11. Goulden, C. H.: Methods of Statistical Analysis. John Wiley & Sons, Inc., 1949.
12. Jones, Eric, and Maslen, K. R.: The Physical Characteristics of Wire Resistance Strain Gauges. Rep. No. Instn. 2, British R.A.E., Nov. 1948.

- CONFIDENTIAL
13. Dobie, W. B., and Isaac, Peter C. G.: Electric Resistance Strain Gages. English Univ. Press, Ltd. (London), 1948.
 14. Crout, Prescott D.: A Short Method for Evaluating Determinants and Solving Systems of Linear Equations With Real or Complex Coefficients. Trans. AIEE, vol. 60, 1941, pp. 1235-1240.
- CONFIDENTIAL

TABLE I
PRELIMINARY AND FINAL CALIBRATION DATA - STRUCTURE A

Station, in.	Rov (fig. 4)	Applied loads		Uncombined bridges										Combined bridges					
		V _i (lb)	M' x 10 ⁻³ (in.-lb)	H _{VRF}	H _{VRM}	H _{VRR}	H _{VLF}	H _{VIM}	H _{VLR}	H _{MRF}	H _{MRM}	H _{MRR}	H _{MLF}	H _{MLM}	H _{MLR}	P _V R	P _V L	P _M R	P _M L
Right side loaded																			
198.5	Front	500	90.15	0.234	0.481	0.270	-0.322	-0.143	-0.223	0.835	0.649	0.980	-0.250	-0.002	-0.194	0.104	-0.017	0.191	-0.013
	Mid	500	90.15	.164	.451	.365	-.303	-.121	-.187	.806	.651	1.009	-.243	-.005	-.177	.106	-.017	.191	-.012
	Rear	500	90.15	.063	.456	.471	-.323	-.121	-.175	.760	.642	1.055	-.254	-.009	-.170	.102	-.017	.191	-.013
130.0	Front	1500	167.63	.881	1.370	.660	-.261	-.122	-.304	1.679	1.219	1.834	-.311	-.044	-.408	.296	-.031	.362	-.023
	Mid	1500	167.63	.516	1.212	1.117	-.359	-.115	-.288	1.537	1.199	2.030	-.374	-.047	-.345	.311	-.031	.362	-.026
	Rear	1500	167.63	.168	1.088	1.254	-.456	-.084	-.189	1.407	1.173	2.196	-.432	-.062	-.293	.327	-.034	.364	-.026
50.0	Front	2500	79.38	1.815	2.803	3.67	0	-.084	-.373	1.163	.563	.731	.062	-.018	-.314	.503	-.015	.179	-.013
	Mid	2500	79.38	1.091	3.401	1.108	-.235	-.108	-.231	.921	.616	.942	-.231	-.004	-.220	.547	-.015	.190	-.013
	Rear	2500	79.38	-.004	1.923	2.670	-.412	-.081	-.016	.589	.520	1.434	-.318	-.019	-.085	.515	-.020	.182	-.015
Left side loaded																			
198.5	Front	500	90.15	-0.473	0.619	-0.310	0.619	0.187	0.637	-0.372	0.060	-0.317	0.958	0.558	1.099	-0.025	0.067	-0.017	0.179
	Mid	500	90.15	-.442	.469	-.211	.525	.181	.707	-.377	.047	-.250	.958	.556	1.087	-.025	.067	-.016	.176
	Rear	500	90.15	-.474	.464	-.183	.459	.171	.759	-.379	.041	-.221	.941	.555	1.114	-.023	.065	-.014	.178
130.0	Front	1500	167.63	-.817	1.055	-.515	1.134	-.266	.624	-.605	.055	-.449	1.834	1.128	1.681	-.053	.208	-.027	.336
	Mid	1500	167.63	-.904	1.050	-.458	.759	-.227	1.155	-.692	.049	-.427	1.733	1.154	1.902	-.056	.210	-.026	.335
	Rear	1500	167.63	-.981	1.014	-.362	.367	-.207	1.616	-.717	.049	-.371	1.941	1.171	2.106	-.055	.217	-.027	.337
50.0	Front	2500	79.38	-.920	2.524	-.450	2.352	-.517	1.641	-.204	.059	-.427	1.452	1.444	.810	-.024	.350	-.016	.162
	Mid	2500	79.38	-.462	1.490	-.210	1.361	-.778	1.267	-.390	.042	-.253	1.085	.534	.946	-.027	.374	-.015	.174
	Rear	2500	79.38	-.725	.413	.059	-.435	-.413	2.823	-.568	.008	-.048	.891	.480	1.401	-.031	.356	-.018	.161
Both sides loaded																			
198.5	Front	500	90.15	-0.036	0.769	0.092	-0.015	-0.177	0.155	0.618	0.663	0.769	0.584	0.623	0.781	0.079	0.044	0.173	0.171
	Mid	500	90.15	-.115	.713	.215	-.150	-.200	.240	.583	.647	.822	.531	.633	.857	.083	.048	.175	.162
	Rear	500	90.15	-.246	.734	.313	-.181	-.142	.422	.504	.644	.856	.524	.629	.906	.087	.048	.175	.163
130.0	Front	1500	167.63	-.379	2.180	0.999	.668	-.386	.418	1.277	1.265	1.264	1.377	1.128	1.424	.258	.167	.328	.306
	Mid	1500	167.63	-.100	2.065	.654	.158	-.397	.936	1.044	1.286	1.504	1.164	1.122	1.625	.268	.174	.332	.311
	Rear	1500	167.63	-.603	1.989	1.185	-.577	-.412	1.456	.832	1.185	1.766	.965	1.113	1.853	.286	.170	.330	.315
50.0	Front	2500	79.38	1.841	3.137	2.181	2.148	-.687	.290	1.103	.593	.247	1.197	.458	.527	.487	.329	.158	.151
	Mid	2500	79.38	.662	3.922	.736	1.099	-.846	1.193	.587	.661	.809	.809	.530	.807	.525	.351	.172	.158
	Rear	2500	79.38	-.679	2.424	2.590	-.016	-.542	2.846	.052	.517	1.325	.533	.454	1.320	.492	.342	.165	.143



TABLE II
SUMMARY OF LOAD COEFFICIENTS AND PROBABLE ERRORS FOR STRUCTURE A

Equation for	Load coefficient, a_{ij} for equation (37)						Probable error of est.
	Preliminary						
V_L	a_{11} 570 ± 10	a_{12} -1300 ± 35	a_{13} 570 ± 10	a_{14} (14 ± 1) × 10 ⁻⁴	a_{16} (8 ± 1) × 10 ⁻⁴		P.E. (V_L), lb 28
M_L	a_{21} 15,700 ± 1570	a_{22} 98,550 ± 4100	a_{23} 14,190 ± 1860	a_{26} (830 ± 70) × 10 ⁻⁴			P.E. (M_L), in.-lb 1967
V_R	a_{41} 700 ± 35	a_{42} 330 ± 20	a_{43} 725 ± 25	a_{44} (-7 ± 2) × 10 ⁻⁴	a_{46} (35 ± 6) × 10 ⁻⁴		P.E. (V_R), lb 42
M_R	a_{51} 12,950 ± 2250	a_{52} 90,400 ± 5650	a_{53} 19,450 ± 1750	a_{56} (750 ± 146) × 10 ⁻⁴			P.E. (M_R), in.-lb 1493
Final							
	Load coefficient, a'_{ij} for equation (39)						
V_L	a'_{11} 6845 ± 45	a'_{12} 295 ± 50		a'_{13} 0	a'_{14} 680 ± 30		P.E. (V_L), lb 28
M_L	a'_{21} -11,280 ± 2150	a'_{22} 509,730 ± 2270		a'_{23} 0	a'_{24} 34,720 ± 1340		P.E. (M_L), in.-lb 1305
V_R	a'_{31} 0	a'_{32} 705 ± 40		a'_{33} 4790 ± 25	a'_{34} 0		P.E. (V_R), lb 37
M_R	a'_{41} 0	a'_{42} 40,810 ± 1170		a'_{43} -14,180 ± 1240	a'_{44} 479,970 ± 1790		P.E. (M_R), in.-lb 1060



TABLE III
 DISTRIBUTED CHECK LOAD DATA FOR STRUCTURE A

Distribution (fig. 10)	Combined bridge response, ρ			
	ρ_{VL}	ρ_{ML}	ρ_{VR}	ρ_{MR}
A ₁	0.266	0.405	0.426	0.443
Shear and moment comparison from equation (39)				
A ₁ Applied Calculated Difference Percent difference	V_L	M_L	V_R	M_R
	2250	226,420	2250	226,420
	2240	228,000	2320	223,000
	10	-1380	-70	-3420
	0.4	-0.6	-3.1	-1.5





TABLE IV.- LEFT STABILIZER SHEAR EQUATIONS FOR STRUCTURE A

(a) Preliminary equations

From table I and equation (31), $\{v_L\} = \{R\} \{a\}$

		w_{VLF}	w_{VLM}	w_{VLR}	$M_L \times 10^{-3}$	$M_R \times 10^{-3}$		
1	$\left\{ \begin{array}{c} 0 \\ 0 \\ \vdots \\ \vdots \\ 500 \\ \vdots \\ \vdots \\ 1500 \\ \vdots \\ \vdots \\ 2500 \end{array} \right\}$	0	-0.322	-0.143	-0.223	0	90.15	
1		0	-0.303	-0.121	-0.187	0	90.15	
2		\vdots	\vdots	\vdots	\vdots	\vdots	\vdots	\vdots
\vdots		\vdots	\vdots	\vdots	\vdots	\vdots	\vdots	\vdots
11		500	0.619	0.187	0.637	90.15	0	a_{11}
\vdots		\vdots	\vdots	\vdots	\vdots	\vdots	\vdots	a_{12}
\vdots		\vdots	\vdots	\vdots	\vdots	\vdots	\vdots	a_{13}
\vdots		\vdots	\vdots	\vdots	\vdots	\vdots	\vdots	a_{14}
23		1500	0.668	-0.386	0.418	167.63	167.63	a_{16}
\vdots		\vdots	\vdots	\vdots	\vdots	\vdots	\vdots	\vdots
\vdots		\vdots	\vdots	\vdots	\vdots	\vdots	\vdots	\vdots
n = 27		2500	-0.016	-0.542	2.846	79.38	79.38	\vdots

$$\left\{ \begin{array}{c} \{R\}^T \{v_L\} \\ \vdots \\ \vdots \\ \vdots \end{array} \right\} = \left\{ \begin{array}{c} 22,839 \\ -12,290 \\ 33,417 \\ 14,848 \times 10^5 \\ 29,697 \times 10^5 \end{array} \right\} \text{ and } \left[\begin{array}{c} \{R\}^T \{R\} \\ \vdots \\ \vdots \\ \vdots \end{array} \right] = \left[\begin{array}{cccccc} 18.051 & -4.831 & 9.650 & -0.5017 \times 10^5 & 11.196 \times 10^5 \\ 4.831 & 3.470 & -6.952 & -5.268 \times 10^5 & -6.161 \times 10^5 \\ 9.650 & -6.652 & 29.422 & 6.403 \times 10^5 & 20.225 \times 10^5 \\ -0.502 \times 10^5 & -5.268 \times 10^5 & 6.403 \times 10^5 & 25.515 \times 10^{10} & 12.758 \times 10^{10} \\ 11.196 \times 10^5 & -6.161 \times 10^5 & 20.225 \times 10^5 & 12.758 \times 10^{10} & 25.515 \times 10^{10} \end{array} \right]$$

Using the step-by-step procedure for solving simultaneous equations given in reference 14

$$\left[\begin{array}{c} \{R\}^T \{R\} \\ \vdots \\ \vdots \\ \vdots \end{array} \right]^{-1} = \left[\begin{array}{ccccc} 0.20062 & 0.42932 & 0.08073 & 0.12868 \times 10^{-5} & -0.11270 \times 10^{-5} \\ 0.42932 & 1.65787 & 0.30066 & 0.38465 \times 10^{-5} & -0.21872 \times 10^{-5} \\ 0.08073 & 0.30066 & 0.13354 & 0.08599 \times 10^{-5} & -0.11168 \times 10^{-5} \\ 0.12868 \times 10^{-5} & 0.38465 \times 10^{-5} & 0.08599 \times 10^{-5} & 0.15392 \times 10^{-10} & -0.10871 \times 10^{-10} \\ -0.11270 \times 10^{-5} & -0.21872 \times 10^{-5} & -0.11168 \times 10^{-5} & -0.10871 \times 10^{-10} & 0.17871 \times 10^{-10} \end{array} \right]$$

From equation (30),

$$\left\{ \begin{array}{c} a_{11} \\ a_{12} \\ a_{13} \\ a_{14} \\ a_{15} \end{array} \right\} = \left[\begin{array}{c} \{R\}^T \{R\} \\ \vdots \\ \vdots \\ \vdots \end{array} \right]^{-1} \left\{ \begin{array}{c} \{R\}^T \{v_L\} \\ \vdots \\ \vdots \\ \vdots \end{array} \right\} = \left\{ \begin{array}{c} 567.5 \\ -1305.5 \\ 571.9 \\ 142.5 \times 10^5 \\ 75.1 \times 10^5 \end{array} \right\}$$

From table I, $\sum v_L^2 = 52,500,000$ and from equation (19),

$$\sum v_L^2 = 52,500,000 - \left[\begin{array}{ccccc} 567.5 & -1305.5 & 571.9 & 142.5 \times 10^5 & 75.1 \times 10^5 \end{array} \right] \left\{ \begin{array}{c} 22,839 \\ -12,290 \\ 33,417 \\ 14,848 \times 10^5 \\ 29,697 \times 10^5 \end{array} \right\} = 37,000$$

From equation (18) for n = 27 and q = 5, the probable error of estimate PE(v_L) = 28 lb.

By using the elements on the principle diagonal of the inverse load matrix $\left[\begin{array}{c} \{R\}^T \{R\} \\ \vdots \\ \vdots \\ \vdots \end{array} \right]^{-1}$ and equation (21), the probable errors in the preliminary load coefficients were

$$\left\{ \begin{array}{c} PE(a_{11}) \\ PE(a_{12}) \\ PE(a_{13}) \\ PE(a_{14}) \\ PE(a_{16}) \end{array} \right\} = 28 \left\{ \begin{array}{c} \sqrt{0.2006} \\ \sqrt{1.6579} \\ \sqrt{0.1335} \\ \sqrt{0.1539 \times 10^{-10}} \\ \sqrt{0.1787 \times 10^{-10}} \end{array} \right\} = \left\{ \begin{array}{c} \pm 12 \\ \pm 36 \\ \pm 10 \\ \pm 11 \times 10^{-5} \\ \pm 12 \times 10^{-5} \end{array} \right\}$$

From equation (32), the calculated attenuation required for electrical combination of the three shear bridges mounted on the left stabilizer were

$$p_{V_L} = \frac{570}{-1300} w_{VLF} + w_{VLM} + \frac{570}{-1300} w_{VLR}$$

Similar procedures were followed to obtain p_{M_L} , p_{V_R} , and p_{M_R}

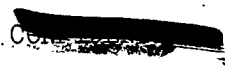


TABLE IV.- LEFT STABILIZER SHEAR EQUATIONS FOR STRUCTURE A - Concluded

(b) Final equations

From table I and equation (33), $\{v_L'\} = \|\rho\| \{a'\}$

i		ρ_{V_L}	ρ_{M_L}	ρ_{M_R}	
1	0	-0.017	-0.013	0.191	$\left\{ \begin{matrix} a'_{11} \\ a'_{12} \\ a'_{14} \end{matrix} \right\}$
2	0	-0.017	-0.120	0.191	
.	
.	
11	500	0.067	0.176	-0.016	
.	
.	
23	1500	0.170	0.315	0.332	
.	
.	
n = 27	2500	0.266	0.405	0.443	

$$\left\{ \|\rho\|^T \{v_L'\} \right\} = \begin{Bmatrix} 7143.5 \\ 5797.0 \\ 2718.0 \end{Bmatrix} \quad \text{and} \quad \left[\|\rho\|^T \|\rho\| \right] = \begin{bmatrix} 0.9836 & 0.7675 & 0.2704 \\ 0.7675 & 0.9586 & 0.3833 \\ 0.2704 & 0.3833 & 1.1094 \end{bmatrix}$$

$$\left[\|\rho\|^T \|\rho\| \right]^{-1} = \begin{bmatrix} 2.71949 & -2.21879 & 0.10379 \\ -2.21879 & 3.02070 & -0.50291 \\ 0.10379 & -0.50291 & 1.04989 \end{bmatrix}$$

$$\left\{ a'_{11} \right\} = \left[\|\rho\|^T \|\rho\| \right]^{-1} \left\{ \|\rho\|^T \{v_L'\} \right\} = \begin{Bmatrix} 6846.4 \\ 294.1 \\ 679.7 \end{Bmatrix}$$

From table I, $\sum v_L'^2 = 52,500,000$ and from equation (19),

$$\sum \epsilon_{v_L}^2 = 52,500,000 - \begin{bmatrix} 6846.4 & 294.1 & 679.7 \end{bmatrix} \begin{Bmatrix} 7143.5 \\ 5797.0 \\ 2718.0 \end{Bmatrix} = 40,419$$

From equation (18) for n = 27 and q = 3, the probable error of estimate PE(v_L) = 28 lb.

By using the elements on the principal diagonal of the inverse matrix $\left[\|\rho\|^T \|\rho\| \right]^{-1}$ and equation (21), the probable errors in the final load coefficients were

$$\left\{ \begin{matrix} PE(a'_{11}) \\ PE(a'_{12}) \\ PE(a'_{14}) \end{matrix} \right\} = 28 \left\{ \begin{matrix} \sqrt{2.7195} \\ \sqrt{3.0207} \\ \sqrt{1.0499} \end{matrix} \right\} = \left\{ \begin{matrix} \pm 46 \\ \pm 49 \\ \pm 29 \end{matrix} \right\}$$

The final left stabilizer shear equation which was used for the evaluation of the flight data was

$$v_L = (6845 \pm 45)\rho_{V_L} + (295 \pm 50)\rho_{M_L} + (680 \pm 30)\rho_{M_R}$$



TABLE V
PRELIMINARY CALIBRATION DATA - STRUCTURE B

Station no.	Row (fig. 11)	Applied loads				Left stabilizer								Right stabilizer							
		V_1 , lb	$M_1' \times 10^{-4}$, in.-lb	$M_2' \times 10^{-4}$, in. lb	$T' \times 10^{-4}$, lb.-in.	${}^H\mu_{LF1}$	${}^H\mu_{LR}$	${}^H\mu_{LF1}$	${}^H\mu_{LR}$	${}^H\mu_{LF2}$	${}^H\mu_{LR}$	${}^H\mu_{FT}$	${}^H\mu_{FB}$	${}^H\mu_{FT}$	${}^H\mu_{FB}$	${}^H\mu_{RT}$	${}^H\mu_{RB}$	${}^H\mu_{VF1}$	${}^H\mu_{VRR}$	${}^H\mu_{RR}$	${}^H\mu_{VF2}$
9	Front	250	1.209	1.309	0.715	0.269	0.383	0.318	0.389	0.154	0.295	0.092	0.136	0.158	0.165	0.271	0.418	0.289	0.398	0.170	0.346
9	Mid	250	1.209	1.373	0.828	0.260	0.446	0.353	0.405	0.137	0.324	0.001	0.041	0.058	0.078	0.259	0.466	0.306	0.406	0.140	0.290
9	Rear	250	1.209	1.463	0.940	0.262	0.469	0.387	0.404	0.134	0.340	0.069	0.026	0.018	0.019	0.258	0.502	0.340	0.422	0.143	0.316
9A	Mid	250	1.153	1.309	0.790	0.254	0.336	0.348	0.378	0.140	0.300	-0.002	0.036	0.046	0.065	0.241	0.434	0.289	0.385	0.132	0.277
8	Front	250	1.102	1.175	0.640	0.257	0.378	0.290	0.347	0.161	0.259	0.093	0.134	0.141	0.151	0.254	0.399	0.248	0.353	0.168	0.239
8	Mid	250	1.102	1.242	0.756	0.244	0.336	0.322	0.362	0.134	0.287	0.003	0.033	0.034	0.055	0.228	0.455	0.275	0.373	0.132	0.263
8	Rear	250	1.102	1.309	0.874	0.230	0.469	0.348	0.367	0.124	0.309	-0.067	-0.032	-0.002	0.002	0.243	0.492	0.304	0.382	0.135	0.290
8A	Mid	250	1.043	1.175	0.719	0.234	0.318	0.299	0.335	0.138	0.264	0.009	0.045	0.039	0.057	0.215	0.428	0.304	0.334	0.130	0.233
7	Front	250	0.988	1.035	0.560	0.247	0.361	0.251	0.307	0.157	0.223	0.101	0.135	0.130	0.131	0.231	0.391	0.248	0.319	0.159	0.208
7	Mid	250	0.988	1.105	0.681	0.236	0.423	0.289	0.320	0.142	0.251	0.007	0.039	0.026	0.047	0.221	0.447	0.247	0.328	0.141	0.227
7	Rear	250	0.988	1.175	0.804	0.233	0.456	0.319	0.321	0.144	0.275	-0.070	-0.034	-0.057	-0.020	0.221	0.489	0.282	0.344	0.131	0.211
7A	Mid	250	0.925	1.035	0.641	0.228	0.318	0.269	0.303	0.144	0.233	0.114	0.046	0.025	0.044	0.216	0.432	0.295	0.309	0.140	0.211
6	Front	500	1.738	1.773	0.955	0.499	0.731	0.422	0.534	0.362	0.380	0.251	0.301	0.287	0.273	0.481	0.767	0.380	0.518	0.365	0.354
6	Mid	500	1.738	1.919	1.210	0.476	0.828	0.512	0.559	0.322	0.447	0.111	0.080	0.023	0.064	0.448	0.859	0.431	0.574	0.315	0.395
6	Rear	500	1.738	2.075	1.463	0.469	0.900	0.578	0.573	0.299	0.498	-0.153	-0.084	-0.160	-0.079	0.428	0.954	0.486	0.596	0.279	0.444
6A	Mid	500	1.613	1.467	0.777	0.466	0.619	0.472	0.520	0.326	0.407	0.022	0.081	0.013	0.050	0.453	0.875	0.398	0.544	0.322	0.368
5	Front	500	1.485	1.467	0.777	0.478	0.696	0.354	0.455	0.375	0.309	0.250	0.296	0.256	0.241	0.452	0.736	0.308	0.460	0.378	0.278
5	Mid	500	1.485	1.619	1.043	0.454	0.808	0.421	0.477	0.338	0.368	0.036	0.094	0.006	0.031	0.425	0.851	0.363	0.493	0.331	0.328
5	Rear	500	1.485	1.773	1.308	0.428	0.883	0.491	0.500	0.281	0.418	-0.148	-0.095	-0.190	-0.125	0.419	0.944	0.444	0.524	0.285	0.382
5A	Mid	500	1.350	1.467	0.954	0.429	0.816	0.385	0.439	0.324	0.320	0.029	0.066	-0.028	-0.008	0.421	0.848	0.333	0.454	0.334	0.300
4	Front	750	1.838	1.722	0.893	0.718	0.991	0.402	0.539	0.634	0.352	0.417	0.481	0.354	0.359	0.678	1.054	0.364	0.542	0.648	0.331
4	Mid	750	1.838	1.960	1.309	0.659	1.204	0.226	0.290	0.532	0.438	0.053	0.124	0.051	-0.027	0.637	1.269	0.447	0.620	0.544	0.390
4	Rear	750	1.838	2.200	1.721	0.609	1.368	0.633	0.619	0.453	0.520	-0.241	-0.185	-0.370	-0.281	0.576	1.443	0.536	0.663	0.446	0.476
4A	Mid	750	1.635	1.722	1.174	0.624	1.219	0.457	0.538	0.737	0.375	0.052	0.123	0.086	0.032	0.611	1.221	0.332	0.532	0.544	0.333
3	Front	750	1.430	1.226	0.608	0.740	0.934	0.276	0.415	0.767	0.223	0.379	0.446	0.254	0.260	0.706	1.024	0.240	0.404	0.754	0.203
3	Mid	750	1.430	1.473	1.039	0.605	1.159	0.370	0.419	0.543	0.298	0.079	0.098	-0.076	0.004	0.598	1.217	0.332	0.453	0.552	0.271
3	Rear	750	1.430	1.722	1.471	0.565	1.322	0.500	0.473	0.453	0.400	-0.266	-0.179	-0.455	-0.305	0.533	1.399	0.429	0.519	0.449	0.361
2	Front	1000	1.338	0.921	0.610	1.190	0.956	0.131	0.372	1.404	0.023	0.397	0.732	0.290	0.264	1.082	1.040	0.122	0.374	1.350	0.033
2	Rear	1000	1.338	1.634	1.610	0.630	1.482	0.432	0.535	0.358	0.367	-0.283	-0.239	-0.553	-0.446	0.625	1.858	0.414	0.448	1.544	0.330
1	Front	1000	0.750	0.215	0	1.250	0.815	-0.085	0.269	1.358	0.184	0.301	0.076	0.222	0.180	1.087	0.905	-0.060	0.206	1.117	-0.153
1	Mid	1000	0.750	0.574	0.625	0.789	1.252	0.095	0.148	0.830	-0.034	0.155	0.147	0.005	-0.421	0.689	1.400	0.097	0.123	0.748	0.019
1	Rear	1000	0.750	0.921	1.250	0.519	1.853	-0.315	0.147	1.442	-0.223	-0.165	-0.091	-0.342	-0.314	0.510	1.850	0.263	0.189	0.451	0.195



TABLE VI
SUMMARY OF PRELIMINARY LOAD COEFFICIENTS AND PROBABLE ERRORS FOR STRUCTURE B - LEFT SIDE

Equation for	Load coefficient, b_{ij} for equation (40)										Probable error of estimate																													
	b_{11}	b_{13}	b_{14}	b_{15}	b_{16}	b_{17}	b_{18}	b_{21}	b_{23}	b_{24}		b_{25}	b_{26}	b_{27}	b_{28}	b_{31}	b_{33}	b_{34}	b_{35}	b_{36}	b_{37}	b_{38}	b_{42}	b_{43}	b_{44}	b_{45}	b_{46}	b_{47}	b_{48}	b_{52}	b_{53}	b_{54}	b_{55}	b_{56}	b_{57}	b_{58}				
V_{L1}	535 ± 12 570 ± 12 545 ± 11 590 ± 13	425 ± 7 410 ± 7 440 ± 8 410 ± 11	-194 ± 8 -200 ± 10 -220 ± 9 -215 ± 15	115 ± 14	67 ± 14	105 ± 13	45 ± 20	2815 ± 350 -1920 ± 330 -2260 ± 310 -882 ± 450	2815 ± 200 2400 ± 190 3600 ± 240 2900 ± 380	28,620 ± 250 28,130 ± 280 27,240 ± 260 26,750 ± 500	5650 ± 440	4650 ± 370	5280 ± 380	4100 ± 670	5490 ± 435 -7185 ± 530 -6475 ± 500 -6865 ± 400	6115 ± 250 7025 ± 310 5725 ± 375 5410 ± 345	17,390 ± 310 17,750 ± 450 18,645 ± 425 20,040 ± 445	-6240 ± 540	-3625 ± 600	-4870 ± 615	-5845 ± 600	410 ± 14 415 ± 15 415 ± 12 455 ± 14	460 ± 9 440 ± 10 480 ± 11 445 ± 14	-33 ± 13 -21 ± 16 -64 ± 14 -37 ± 21	125 ± 22	41 ± 22	125 ± 18	46 ± 26	410 ± 14 415 ± 15 415 ± 12 455 ± 14	3570 ± 290 3960 ± 150 3780 ± 350 3300 ± 380	32,200 ± 400 31,735 ± 380 31,950 ± 460 32,480 ± 570	310 ± 680	1740 ± 660	660 ± 610	-400 ± 710	440 400 430 450	440 400 430 450	440 400 430 450	440 400 430 450	
M_{L1}																																								
T_{L1}																																								
V_{L2}																																								
M_{L2}																																								

* Equations used for determining combining ratios.



TABLE VII
 SUMMARY OF PRELIMINARY LOAD COEFFICIENTS AND PROBABLE ERRORS
 FOR STRUCTURE B - RIGHT SIDE

Equation for	Load coefficients, b_{ij} for equation (42)			Probable error of estimate, P.E.
V_{R1}	b_{11} 655 ± 10	b_{13} 380 ± 5	b_{14} -225 ± 10	P.E. (V_{R1}), lb 10
M_{R1} *	b_{21} 3150 ± 525 3165 ± 375	b_{23} 10 ± 175 -----	b_{24} 27,240 ± 490 27,245 ± 435	P.E. (M_{R1}), in.-lb 557 548
T_{R1}	b_{31} -10,635 ± 495	b_{33} 7990 ± 85	b_{34} 17,075 ± 450	P.E. (T_{R1}), lb-in. 509
V_{R2} *	b_{42} 495 ± 15 495 ± 15	b_{43} 420 ± 10 395 ± 8	b_{44} -50 ± 17 -----	P.E. (V_{R2}) 20 21
M_{R2}	b_{52} -4675 ± 300	b_{53} 2700 ± 215	b_{54} 31,565 ± 350	P.E. (M_{R2}) 403



*Equation used for determining combining ratios.

TABLE VIII

FINAL CALIBRATION DATA FOR STRUCTURE B

Station no.	Row (fig. 11)	Applied load				Left stabilizer					Right stabilizer				
		V', lb	M ₁ ' × 10 ⁻⁴ , in.-lb	M ₂ ' × 10 ⁻⁴ , in.-lb	T' × 10 ⁻⁴ , lb-in.	P _V L ₁	P _V L ₂	P _M L ₁	P _M L ₂	P _T L ₁	P _V R ₁	P _V R ₂	P _M R ₁	P _M R ₂	P _T R ₁
Left side loaded															
9	Rear	250	1.209	1.463	0.940	0.387	0.490	0.364	0.358	0.452	-0.039	-0.028	0.010	0.029	0.079
9	Front	250	1.209	1.309	.715	.383	.477	.373	.358	.337	-.011	0	.007	.014	.023
8	Rear	250	1.102	1.309	.874	.390	.489	.326	.335	.418	-.039	-.019	.009	.030	.077
7	Rear	250	.988	1.175	.804	.384	.489	.292	.321	.385	-.038	-.018	.006	.024	.072
7	Front	250	.988	1.035	.560	.376	.473	.303	.293	.266	.001	.007	.007	.010	.013
6	Rear	500	1.738	1.773	.955	.770	.966	.521	.267	.723	-.068	-.037	.015	.046	.126
5	Rear	500	1.485	1.773	1.308	.762	.963	.443	.524	.650	-.060	-.033	.014	.046	.117
5	Front	500	1.485	1.467	.777	.754	.931	.444	.150	.348	.018	.016	.002	-.007	-.026
4	Rear	750	1.838	2.200	1.721	1.130	1.422	.558	.374	.877	-.076	-.038	.016	.052	.139
3	Rear	750	1.430	1.722	1.471	1.133	1.425	.426	.573	.754	-.070	-.035	.016	.047	.128
3	Front	750	1.430	1.226	.608	1.117	1.385	.419	.449	.282	.056	.038	.001	-.027	-.092
2	Rear	1000	1.338	1.634	1.610	1.488	1.843	.414	.300	.820	-.072	-.037	.015	.049	.137
2	Front	1000	1.338	.921	.411	1.505	1.858	.408	.443	.248	.103	.070	-.009	-.059	-.179
1	Rear	1000	.750	.921	1.250	1.481	1.756	.262	.214	.558	-.059	-.032	.010	.037	.103
1	Front	1000	.750	.215	0	1.479	1.603	.262	.266	.171	.120	.075	-.013	-.074	-.218
Right side loaded															
9	Rear	250	1.209	1.463	0.940	-0.033	-0.003	0.036	0.040	0.020	0.325	0.438	0.368	0.358	0.401
9	Front	250	1.209	1.309	.715	-.004	.002	.013	.010	.008	.301	.399	.345	.333	.355
8	Rear	250	1.102	1.309	.874	-.025	-.005	.032	.033	.019	.324	.441	.337	.332	.386
7	Rear	250	.988	1.175	.804	-.025	-.003	.028	.032	.012	.324	.431	.286	.297	.354
7	Front	250	.988	1.035	.560	0	.002	.004	.004	.002	.289	.392	.278	.266	.297
6	Rear	500	1.738	1.773	.955	-.046	-.009	.050	.054	.024	.640	.874	.532	.518	.645
5	Rear	500	1.485	1.773	1.308	-.039	-.007	.044	.046	.021	.653	.874	.457	.450	.572
5	Front	500	1.485	1.467	.777	.017	.012	-.005	-.006	.002	.594	.806	.417	.380	.438
4	Rear	750	1.838	2.200	1.721	-.047	-.008	.054	.057	.024	.942	1.292	.581	.576	.788
3	Rear	750	1.430	1.722	1.471	-.044	-.009	.050	.054	.024	.978	1.312	.465	.455	.665
3	Front	750	1.430	1.226	.608	.043	.014	-.033	-.039	-.009	.909	1.259	.388	.300	.348
2	Rear	1000	1.338	1.634	1.610	-.046	-.009	.050	.055	.025	1.270	1.691	.429	.440	.789
2	Front	1000	1.338	.921	.411	.087	.034	-.057	-.075	-.021	1.242	1.744	.413	.238	.216
1	Rear	1000	.750	.921	1.250	-.034	.001	.039	.042	.019	1.219	1.576	.186	.219	.615
1	Front	1000	.750	.215	0	.088	.023	-.079	-.090	-.031	1.292	1.474	.311	.105	-.097
Both sides loaded															
9	Rear	250	1.209	1.463	0.940	0.357	0.489	0.382	0.381	0.462	0.277	0.405	0.384	0.398	0.498
9	Front	250	1.209	1.309	.715	.389	.494	.380	.344	.341	.288	.402	.357	.352	.387
8	Rear	250	1.102	1.309	.874	.356	.486	.355	.350	.433	.204	.401	.338	.354	.447
7	Rear	250	.988	1.175	.804	.352	.479	.313	.315	.393	.283	.406	.303	.318	.417
7	Front	250	.988	1.035	.560	.388	.481	.309	.276	.275	.297	.402	.288	.278	.315
6	Rear	500	1.738	1.773	.955	.719	.950	.564	.567	.738	.578	.822	.558	.587	.780
5	Rear	500	1.485	1.773	1.308	.714	.954	.488	.498	.680	.592	.830	.495	.520	.720
5	Front	500	1.485	1.467	.777	.770	.935	.452	.377	.360	.615	.821	.414	.375	.422
4	Rear	750	1.838	2.200	1.721	1.093	1.438	.608	.627	.921	.890	1.272	.601	.630	.932
3	Rear	750	1.430	1.722	1.471	1.073	1.397	.465	.490	.775	.909	1.266	.486	.486	.777
3	Front	750	1.430	1.226	.608	1.151	1.411	.392	.268	.282	.964	1.269	.376	.268	.264
2	Rear	1000	1.338	1.634	1.610	1.415	1.804	.468	.504	.860	1.212	1.670	.429	.477	.912
2	Front	1000	1.338	.921	.411	1.542	1.930	.347	.142	.231	1.326	1.794	.418	.193	.057
1	Rear	1000	.750	.921	1.250	1.416	1.737	.295	.303	.572	1.144	1.528	.190	.253	.704
1	Front	1000	.750	.215	0	1.545	1.644	.182	.004	.149	1.369	1.515	.279	.032	-.298

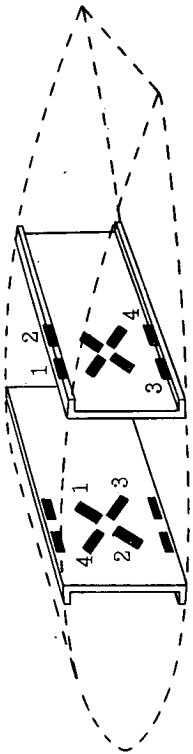
TABLE IX
 SUMMARY OF FINAL LOAD COEFFICIENTS AND
 PROBABLE ERRORS FOR STRUCTURE B

Final equation for	Load coefficients, b'_{ij} for equation (45)					Probable error of estimate, P.E.
V_{L1}	b'_{11} 670 ± 2	b'_{16} 0	b'_{17} -90 ± 15	b'_{18} 90 ± 10		P.E. (V_{L1}), lb 10
M_{L1}	b'_{22} 33,345 ± 235	b'_{26} 525 ± 190	b'_{27} 2440 ± 590	b'_{28} -4045 ± 325		P.E. (M_{L1}), in.-lb 429
T_{L1}	b'_{33} 18,915 ± 370	b'_{36} 0	b'_{37} 0	b'_{38} 0		P.E. (T_{L1}), lb-in. 873
V_{L2}	b'_{44} 576 ± 5	b'_{45} -112 ± 15	b'_{46} 0	b'_{47} 0	b'_{48} 0	P.E. (V_{L2}), lb 17
M_{L2}	b'_{55} 39,225 ± 900	b'_{56} 0	b'_{57} 5070 ± 1980	b'_{58} -5820 ± 1160		P.E. (M_{L2}), in.-lb 1470
V_{R1}	b'_{61} 0	b'_{62} -200 ± 25	b'_{63} 200 ± 20	b'_{66} 785 ± 5		P.E. (V_{R1}), lb 18
M_{R1}	b'_{71} 0	b'_{72} 0	b'_{73} 0	b'_{77} 32,315 ± 325		P.E. (M_{R1}), in.-lb 605
T_{R1}	b'_{81} 0	b'_{82} 0	b'_{83} -1670 ± 430	b'_{86} 2430 ± 565	b'_{88} 16,545 ± 565	P.E. (T_{R1}), lb-in. 1017
V_{R2}	b'_{91} 0	b'_{92} -115 ± 30	b'_{93} 95 ± 25	b'_{99} 605 ± 5		P.E. (V_{R2}), lb 22
M_{R2}	$b'_{10,1}$ 0	$b'_{10,2}$ 7300 ± 1215	$b'_{10,3}$ -6665 ± 905	$b'_{10,10}$ 36,965 ± 475		P.E. (M_{R2}), in.-lb 822

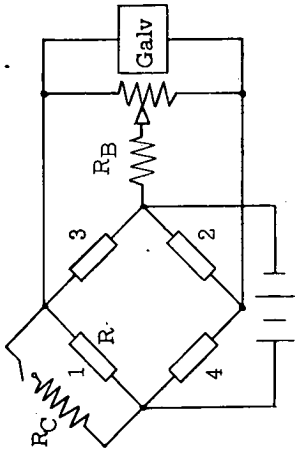
TABLE X
DISTRIBUTED CHECK LOAD DATA FOR STRUCTURE B

Distribution (fig. 21)	Combined bridge response, ρ											
	PV_{L1}	PM_{L1}	PT_{L1}	PV_{L2}	PM_{L2}	PV_{R1}	PM_{R1}	PT_{R1}	PV_{R2}	PM_{R2}	PV_{R2}	PM_{R2}
B1	-1.924	-1.273	-1.321	-2.524	-1.140	-1.571	-1.175	-1.337	-2.201	-1.106		
B2	-1.896	-1.240	-1.303	-2.535	-1.107	-0.795	-0.583	-0.673	-1.101	-0.552		
B3	-0.927	-0.617	-0.663	-1.221	-0.565	-1.578	-1.147	-1.305	-2.200	-1.082		
Shear, moment, and torque comparison from equation (45)												
	V_{L1}	M_{L1}	T_{L1}	V_{L2}	M_{L2}	V_{R1}	M_{R1}	T_{R1}	V_{R2}	M_{R2}	V_{R2}	M_{R2}
B1 Applied	-1300	-38,350	-25,580	-1300	-40,800	-1300	-38,350	-25,580	-1300	-40,800	-1300	-40,800
B1 Calculated	-1299	-40,736	-24,992	-1326	-42,883	-1242	-37,955	-23,723	-1242	-41,378	-1242	-41,378
B1 Difference	1	-2386	592	-26	-2083	58	395	1857	58	-578	58	-578
B1 Percent difference	-0.1	6.2	-2.3	2.0	5.1	-4.5	-1.0	-7.3	-4.5	1.4	-4.5	1.4
B2 Applied	-1300	-38,350	-25,580	-1300	-40,800	-650	-19,175	-12,792	-650	-20,400	-650	-20,400
B2 Calculated	-1275	-40,464	-24,642	-1336	-42,459	-634	-18,830	-10,890	-634	-20,777	-634	-20,777
B2 Difference	25	2114	942	-36	-1659	16	345	1902	16	-377	16	-377
B2 Percent difference	-2.0	5.5	-3.7	2.8	4.1	-2.5	-1.8	-14.9	-2.5	1.9	-2.5	1.9
B3 Applied	-650	-19,175	-12,792	-650	-20,400	-1300	-38,350	-25,584	-1300	-40,800	-1300	-40,800
B3 Calculated	-635	-18,930	-12,543	-640	-20,393	-1250	-37,073	-24,315	-1250	-40,093	-1250	-40,093
B3 Difference	15	245	249	10	7	50	1277	1269	50	707	50	707
B3 Percent difference	-2.3	-1.3	-2.0	-1.5	0	-3.9	-3.3	-5.0	-3.9	-1.7	-3.9	-1.7

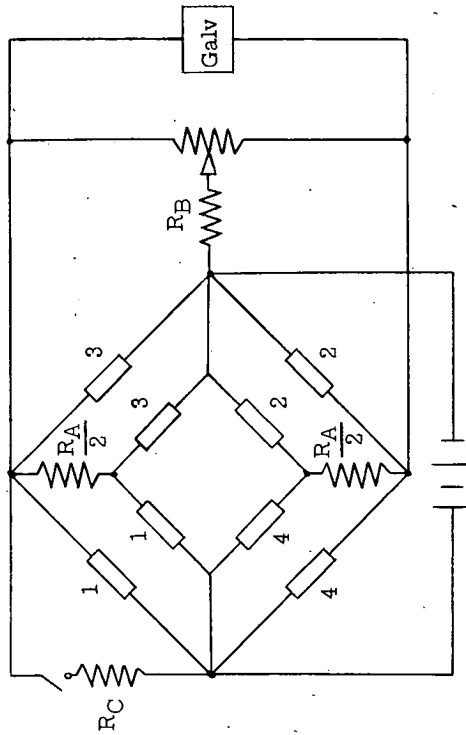




(a) Typical strain-gage installation of shear and moment bridges.



(b) Electrical circuit diagram for a single four-active-arm bridge.



(c) Electrical circuit diagram for two bridges combined.

Figure 1.- Typical strain-gage installation and electrical circuit diagram for a single four-active-arm bridge and two bridges combined.



~~SECRET~~

✕ Shear bridge
= Moment bridge

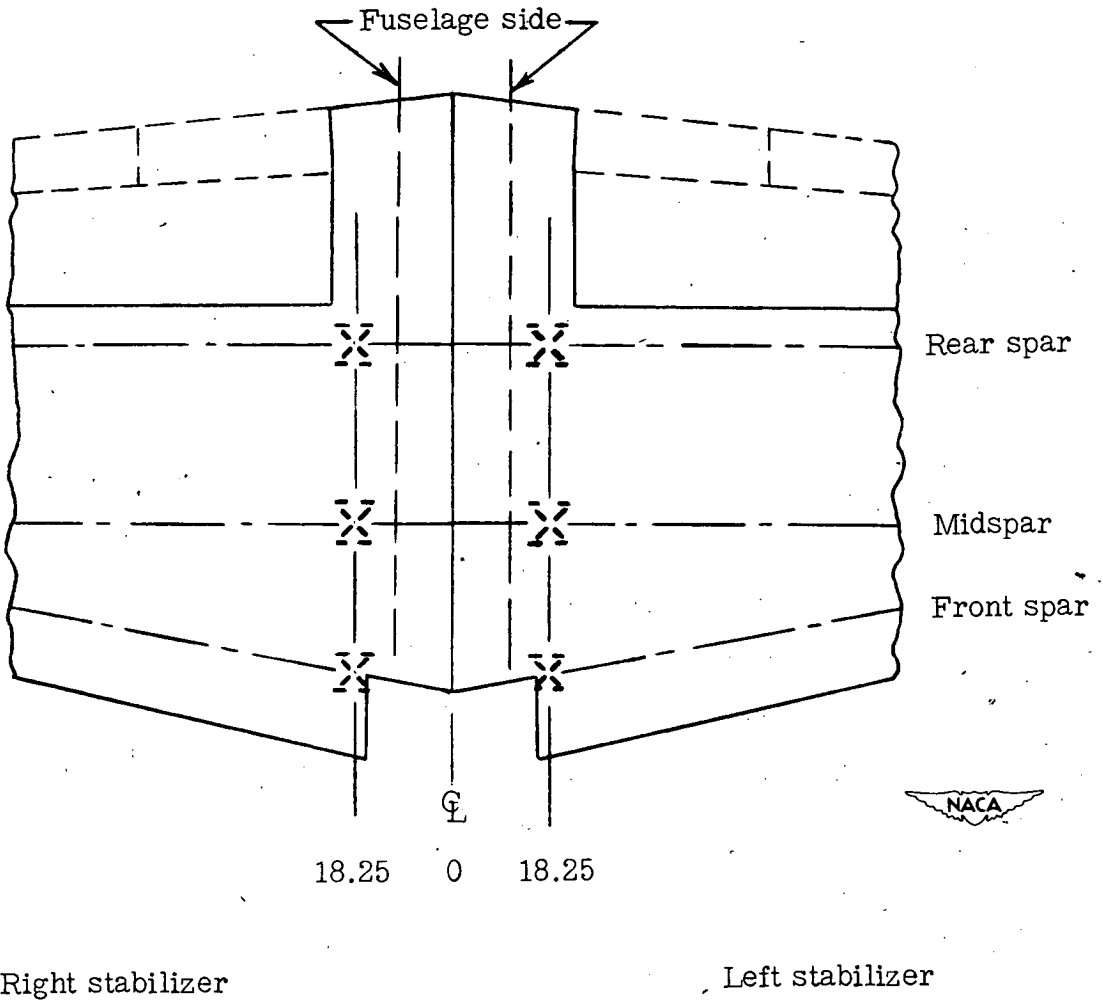


Figure 2.- Strain-gage bridge locations for structure A.

X Shear and torque bridges
 - - - Moment bridges

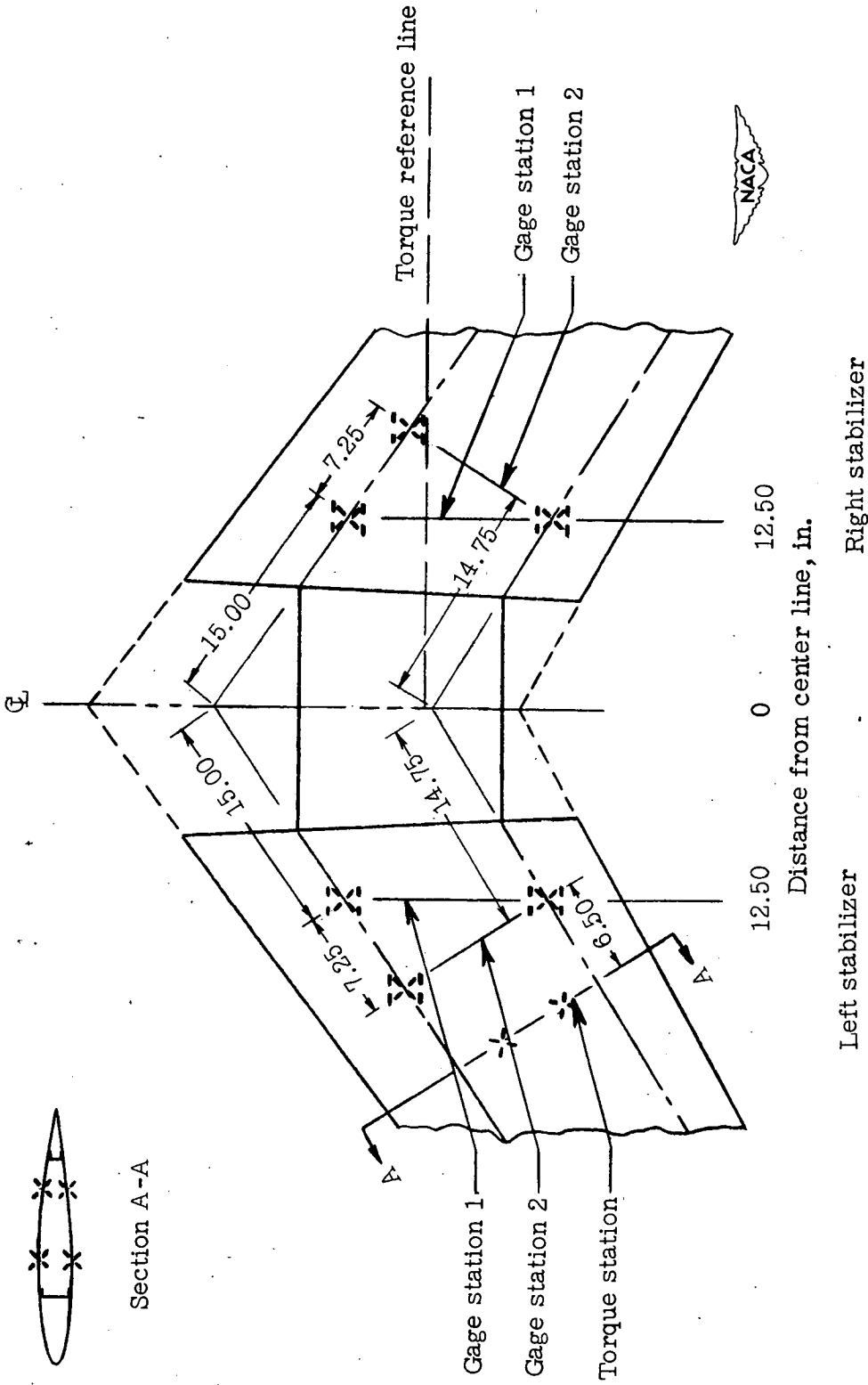


Figure 3.- Strain-gage bridge locations for structure B.

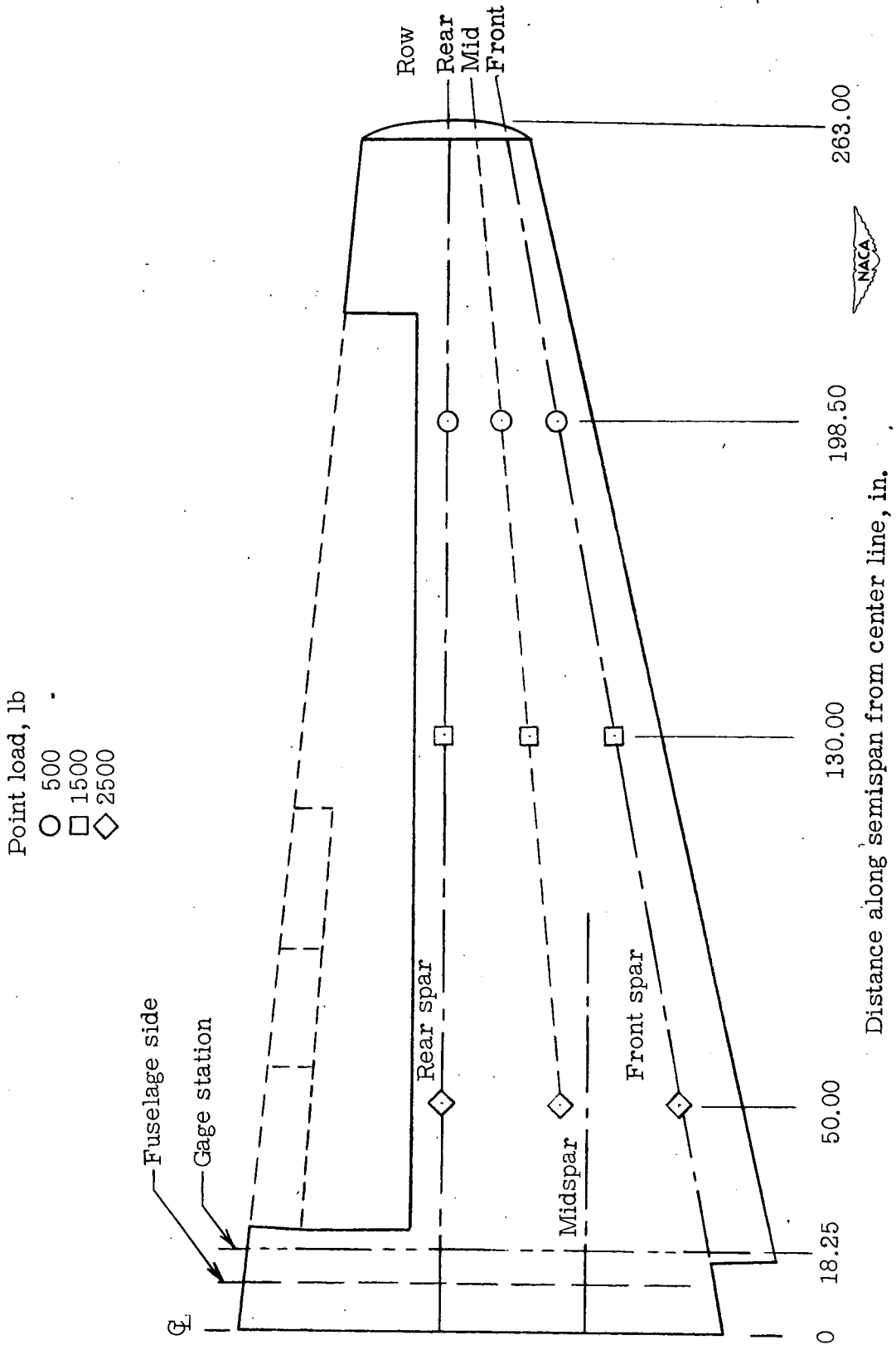


Figure 4.- Loading points for structure A.

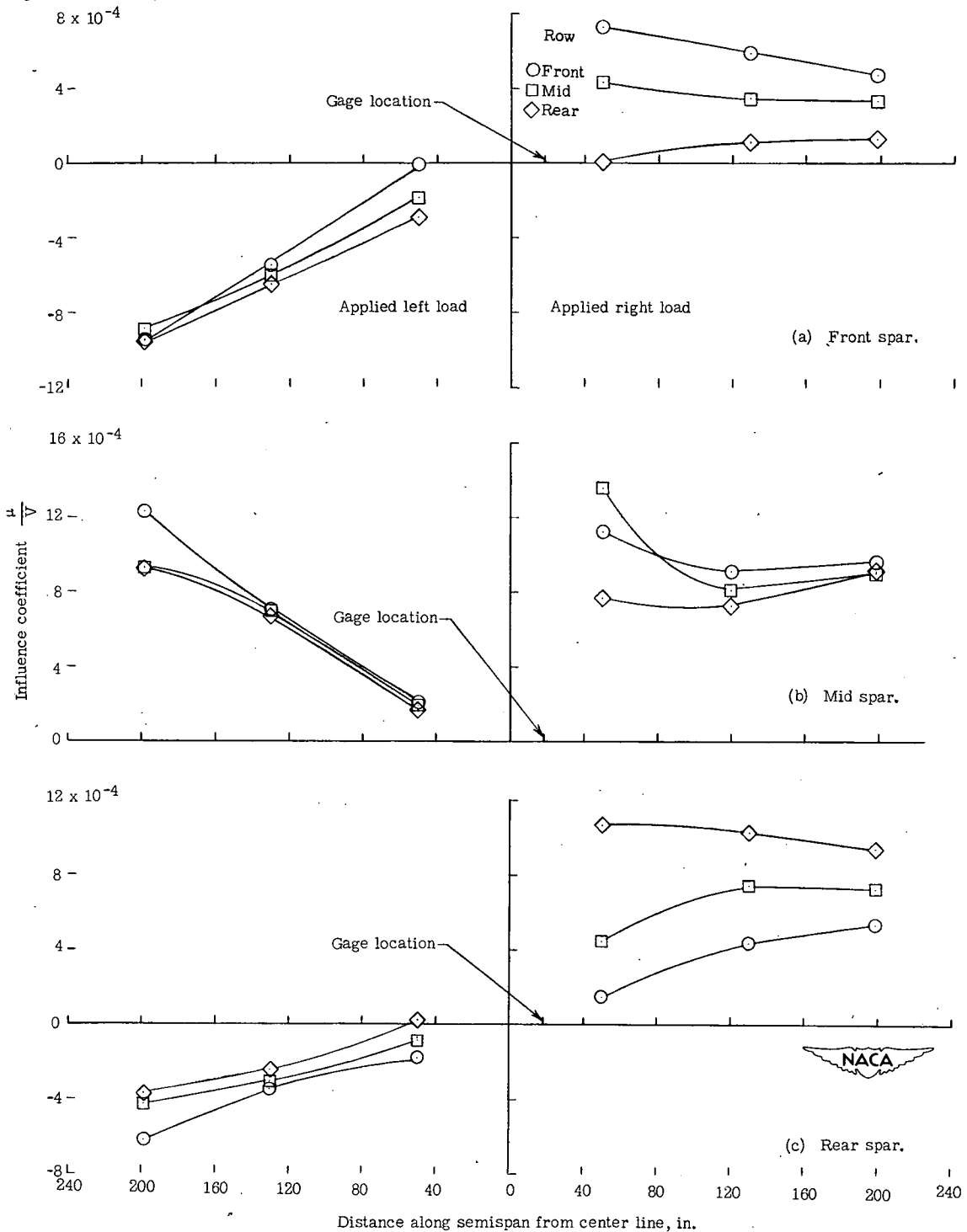


Figure 5.- Influence coefficients for structure A - uncombined right shear bridges.

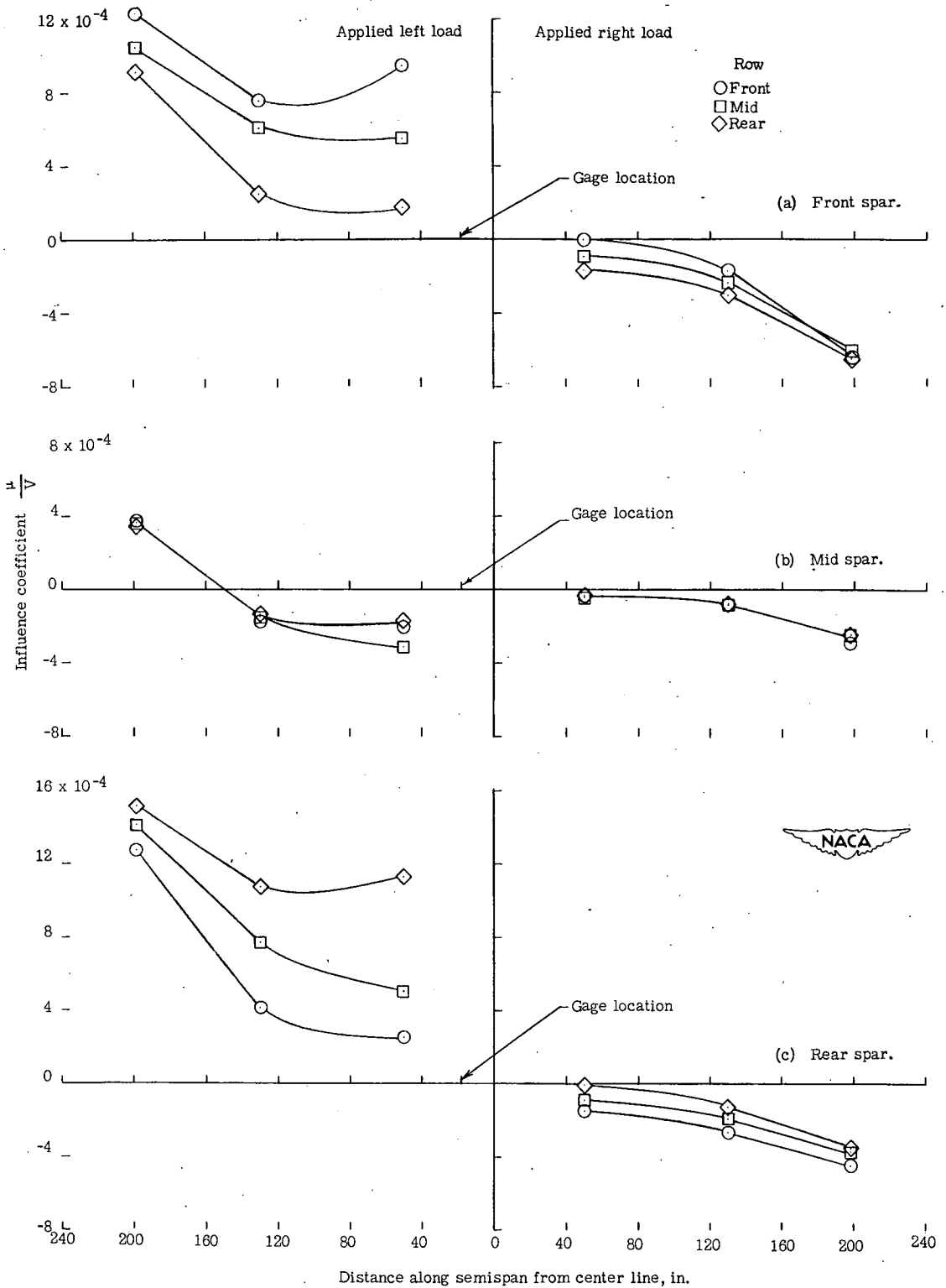


Figure 6.- Influence coefficients for structure A - uncombined left shear bridges.

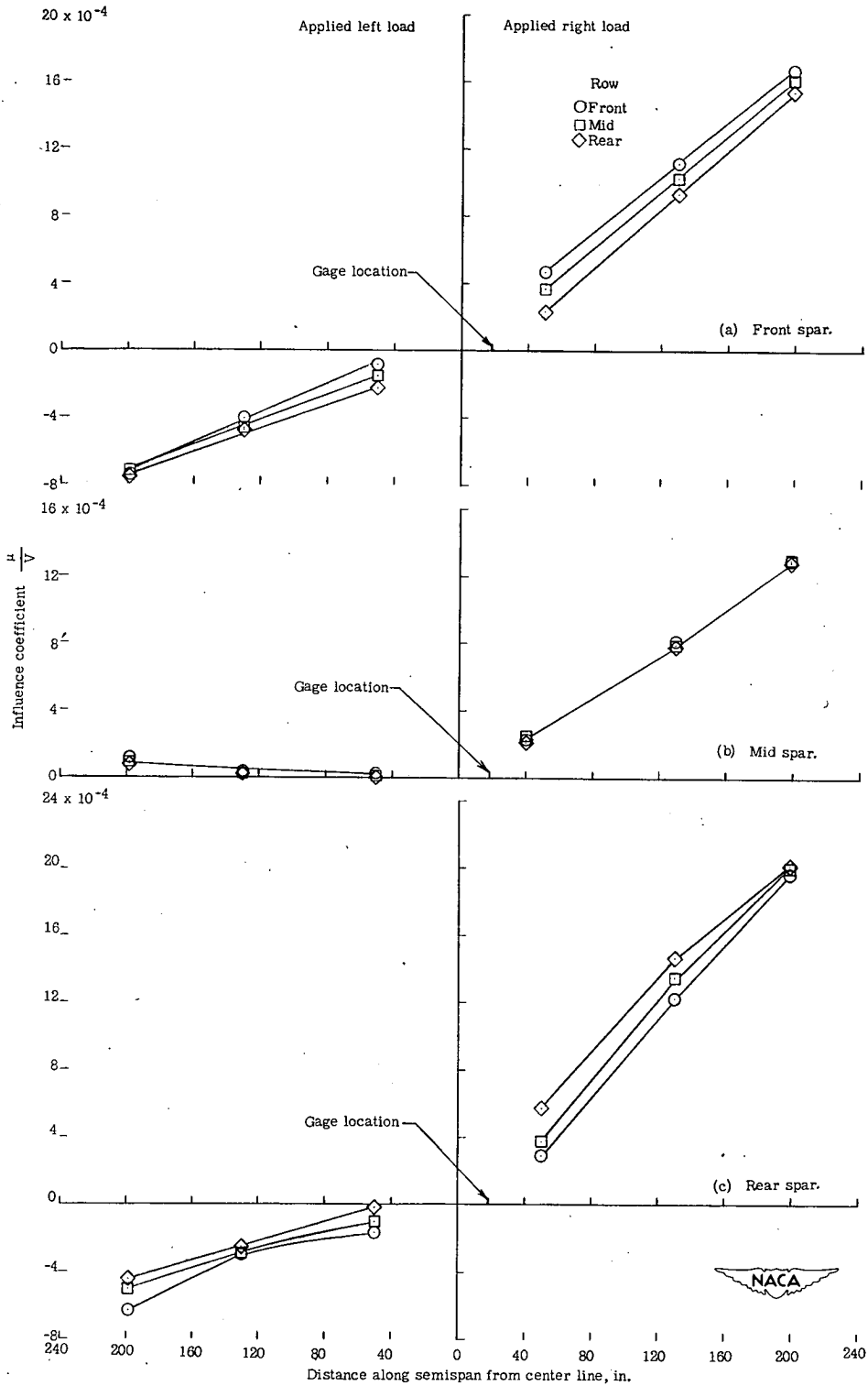


Figure 7.- Influence coefficients for structure A - uncombined right moment bridges.

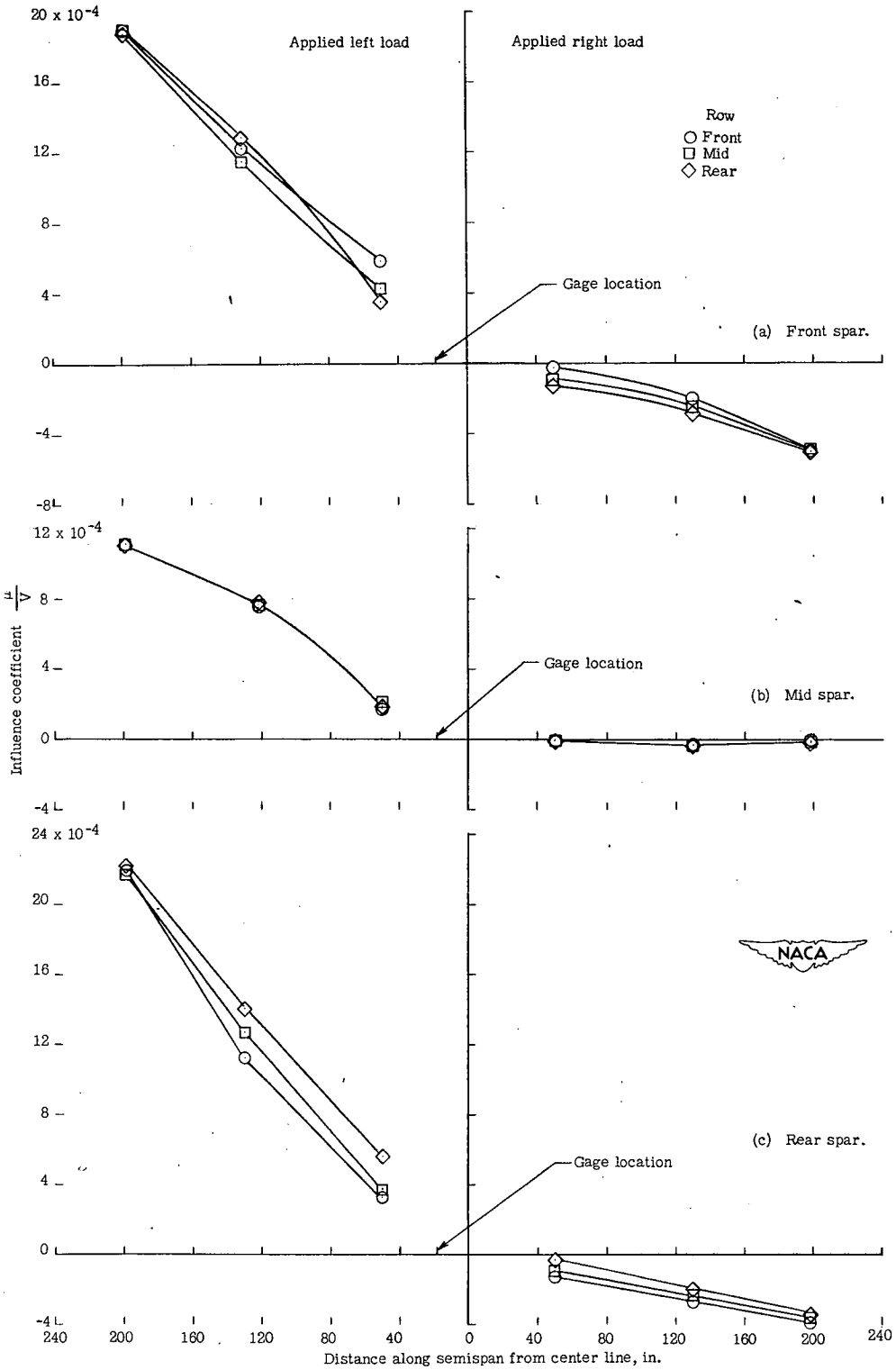


Figure 8.- Influence coefficients for structure A - uncombined left moment bridges.

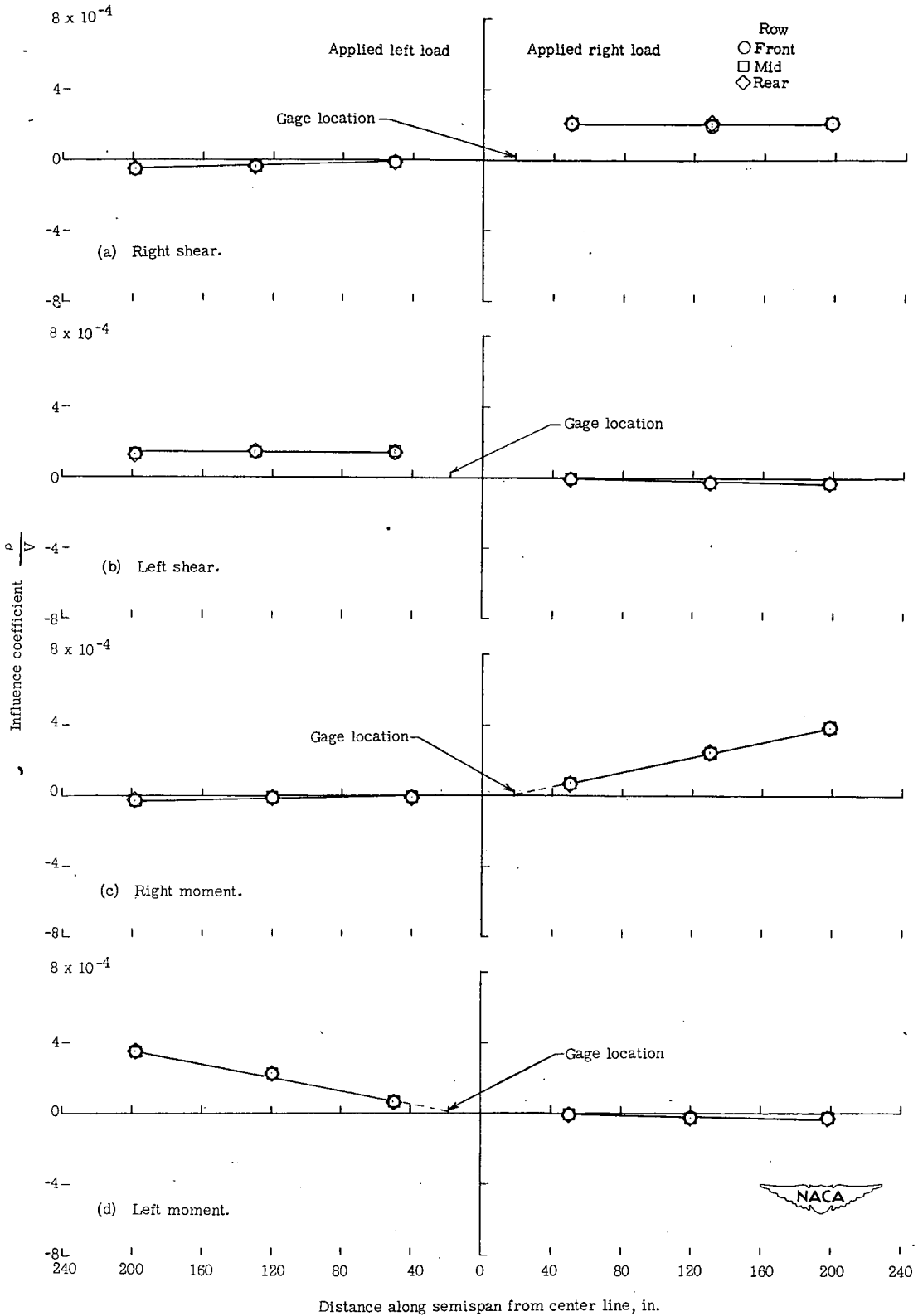
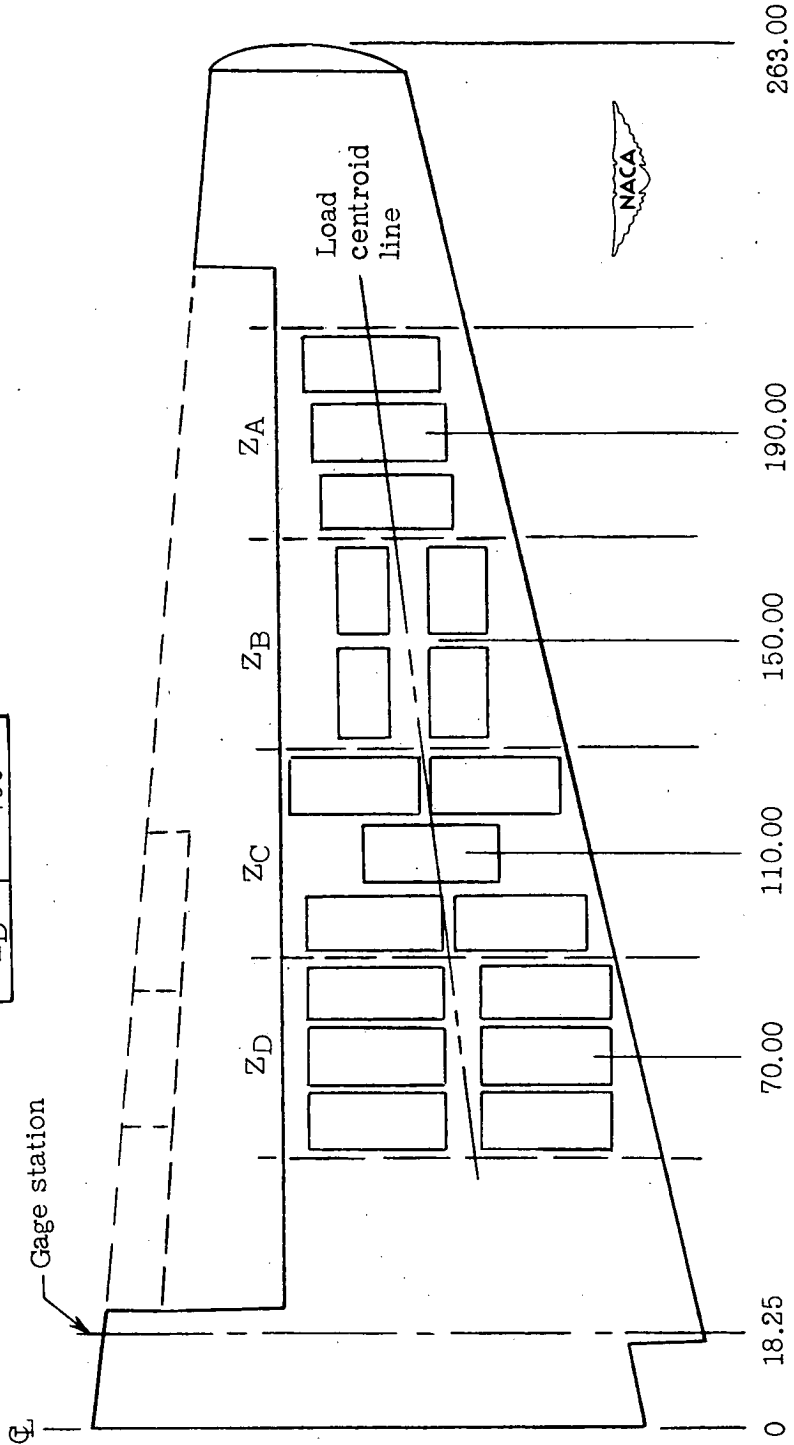


Figure 9.- Influence coefficients for structure A - combined bridges

Distance along chord from L.E. to
load centroid = 44.2 - 0.137y

Loading zones	Applied load, lb
ZA	375
ZB	500
ZC	625
ZD	750



Distance along semispan from center line, in.

Figure 10.- Symmetrical distributed check load A, applied on structure A.

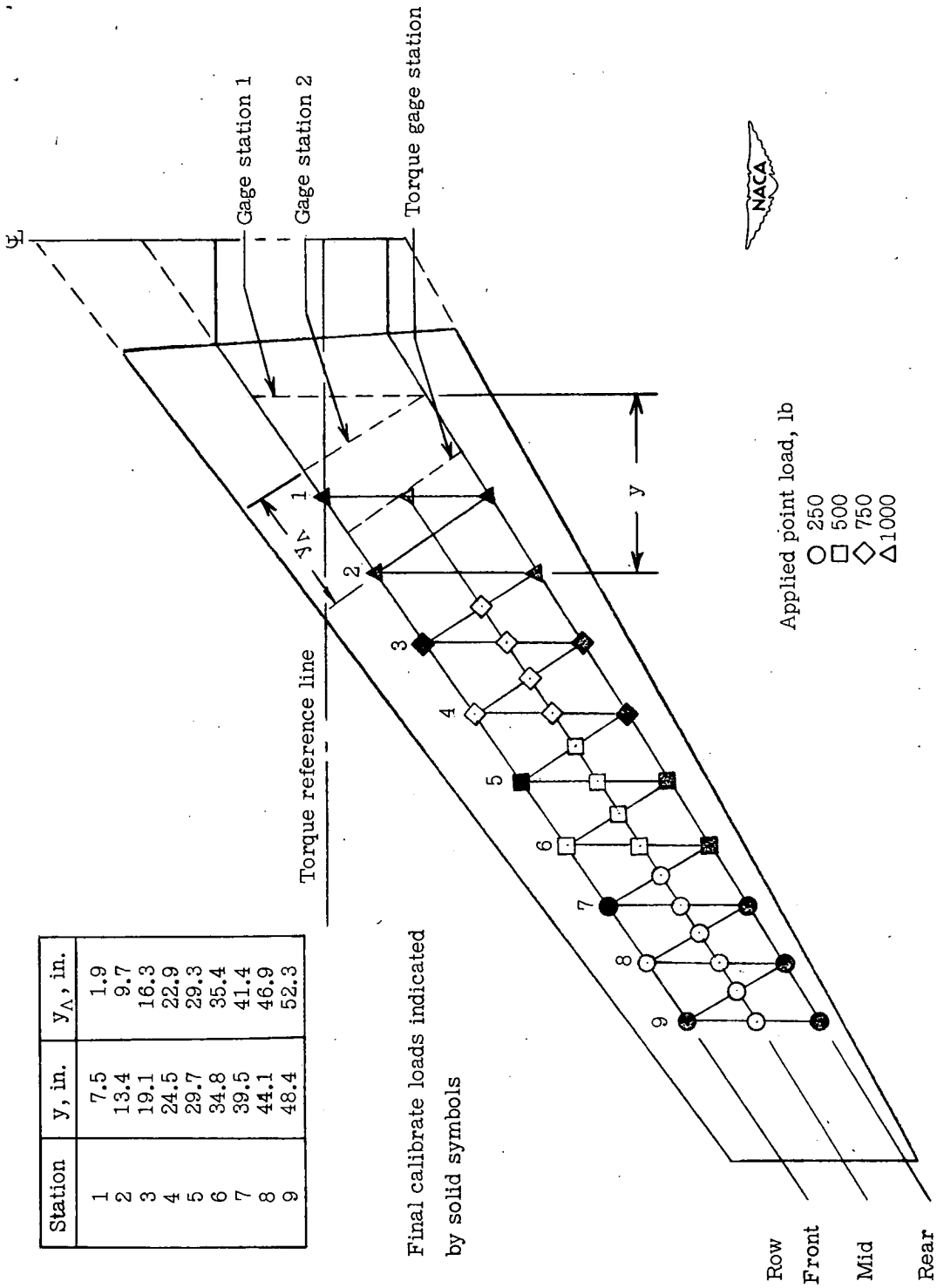


Figure 11.- Loading points for structure B.

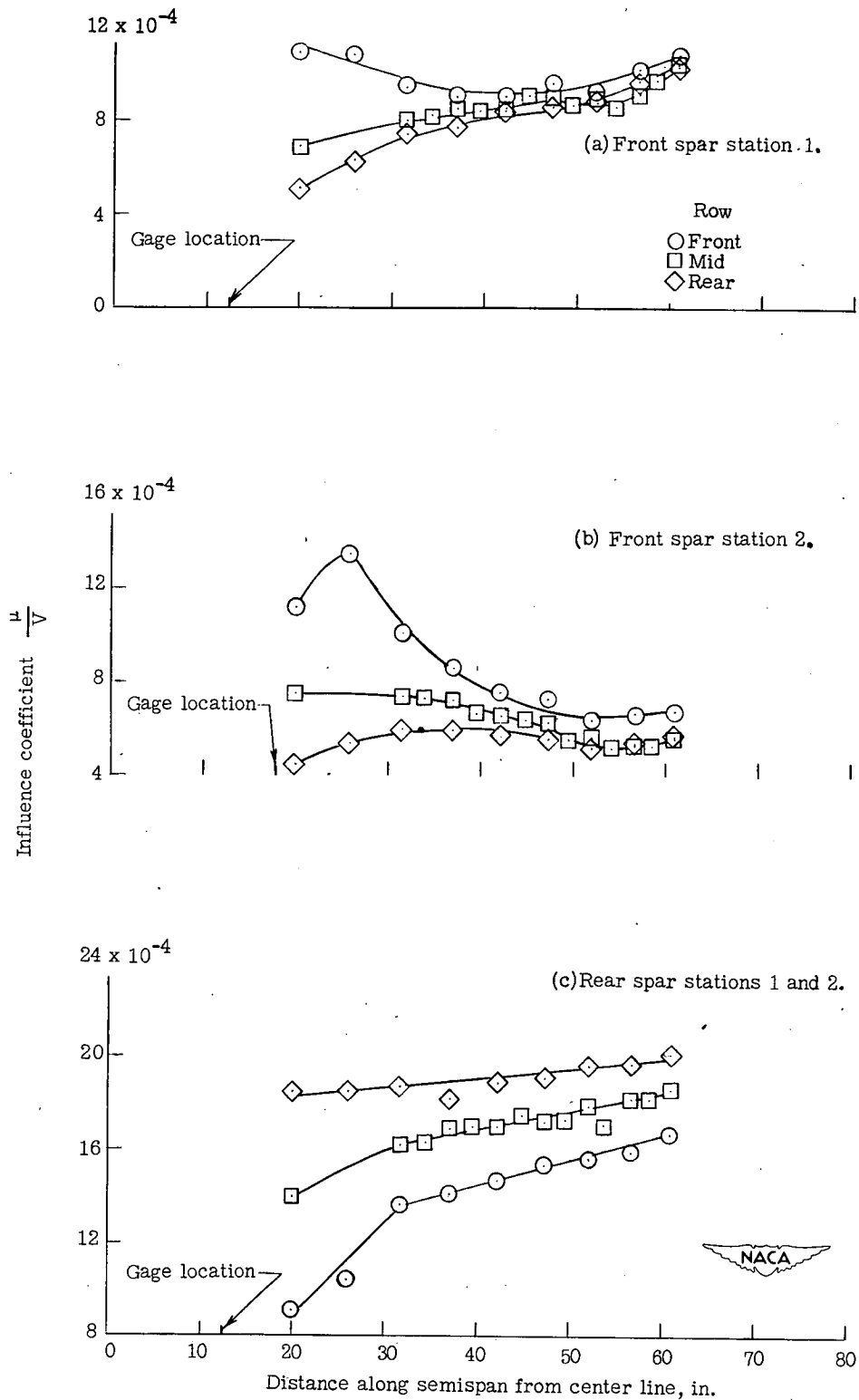


Figure 12.- Influence coefficients for structure B - uncombined right shear bridges.

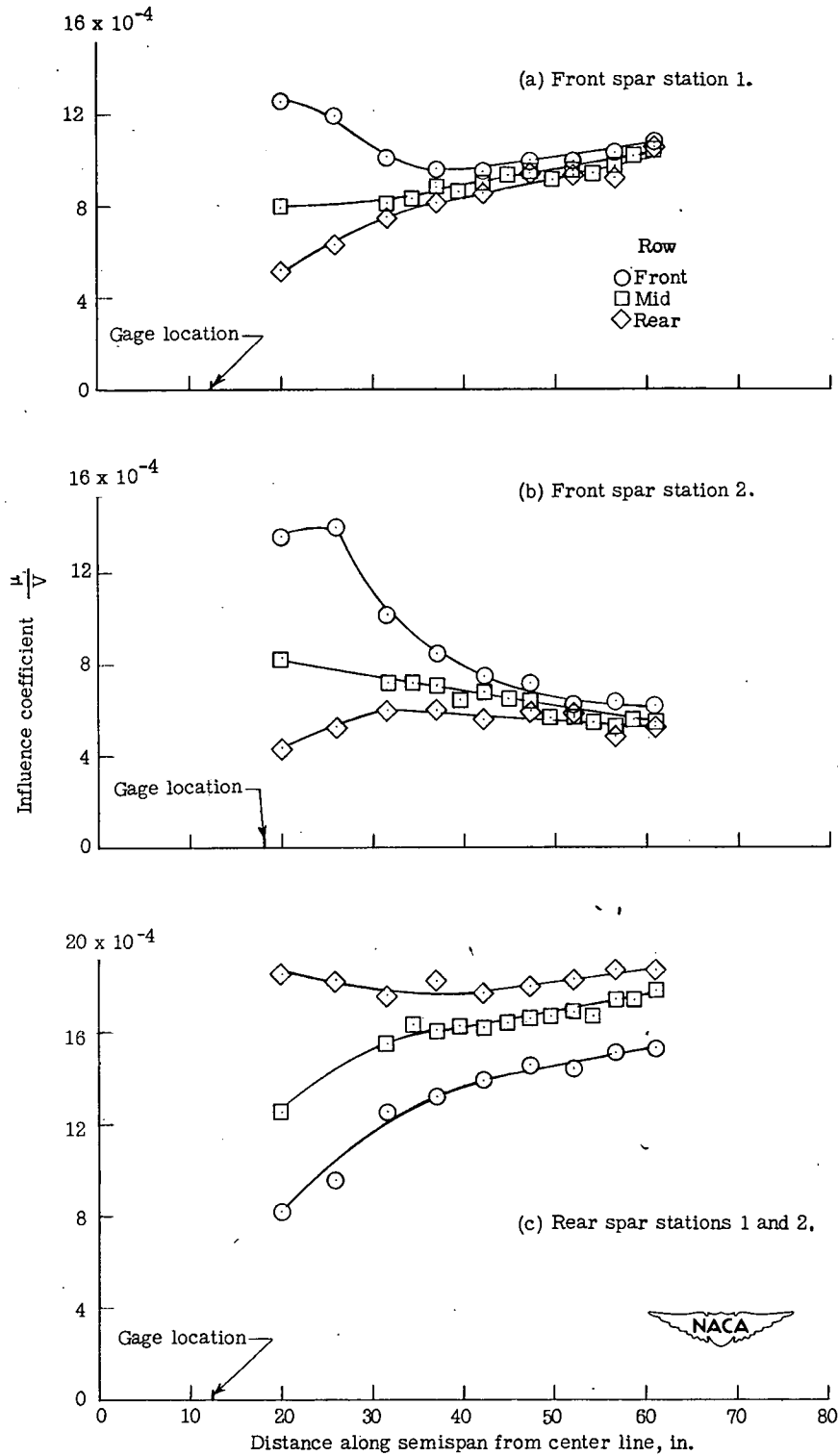


Figure 13.- Influence coefficients for structure B - uncombined left shear bridges.

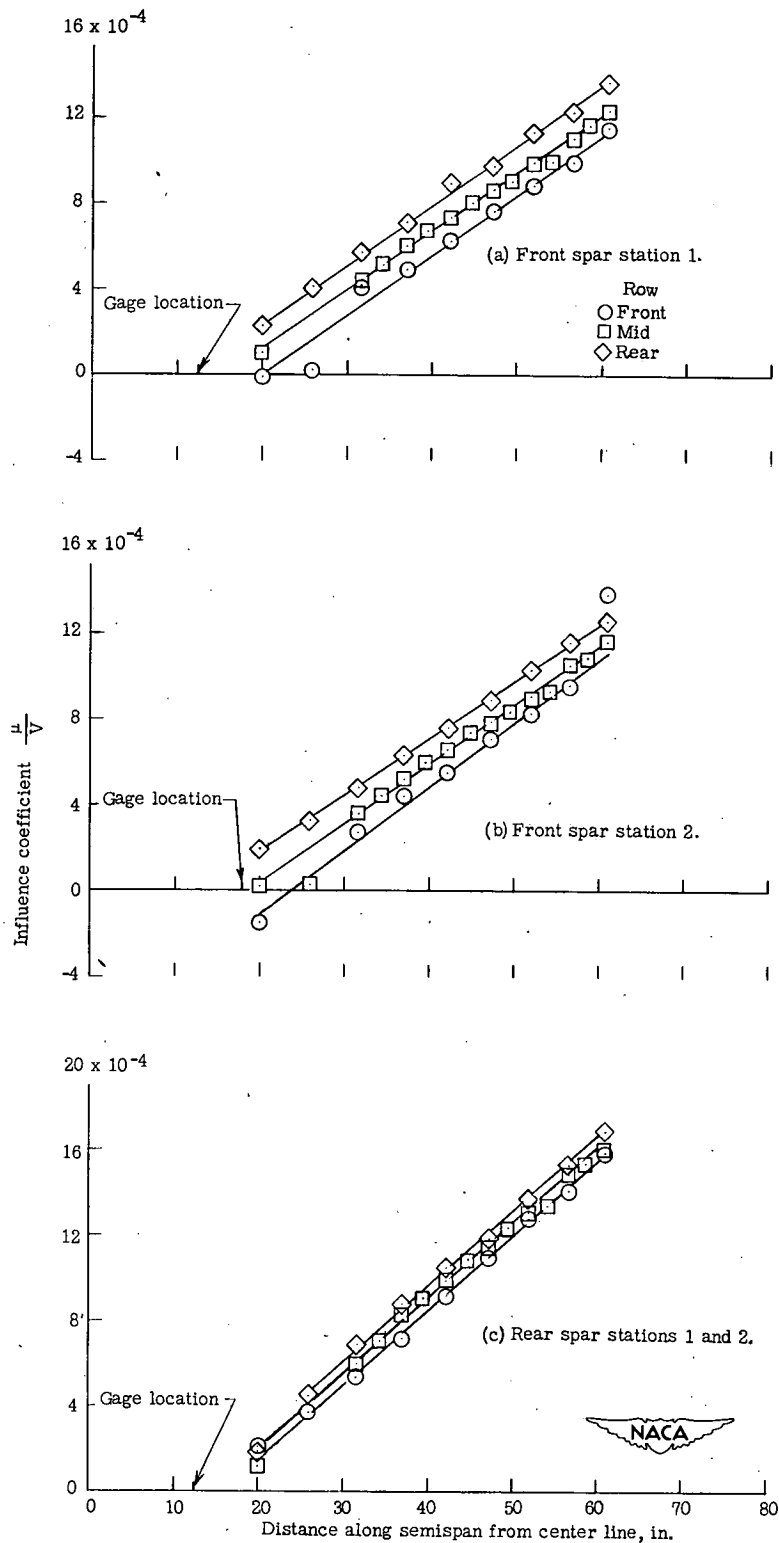


Figure 14.- Influence coefficients for structure B - uncombined right moment bridges.

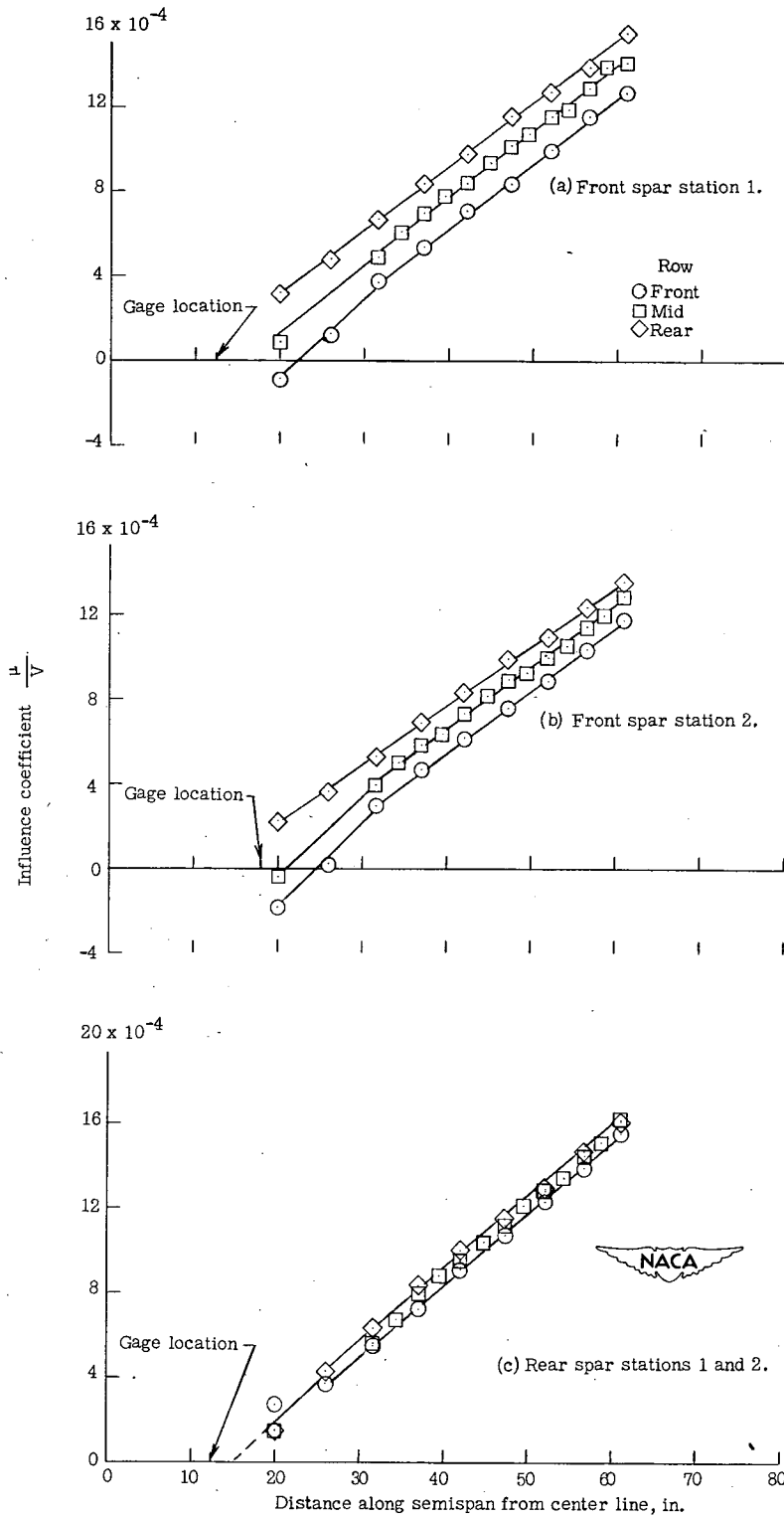


Figure 15.- Influence coefficients for structure B - uncombined left moment bridges.

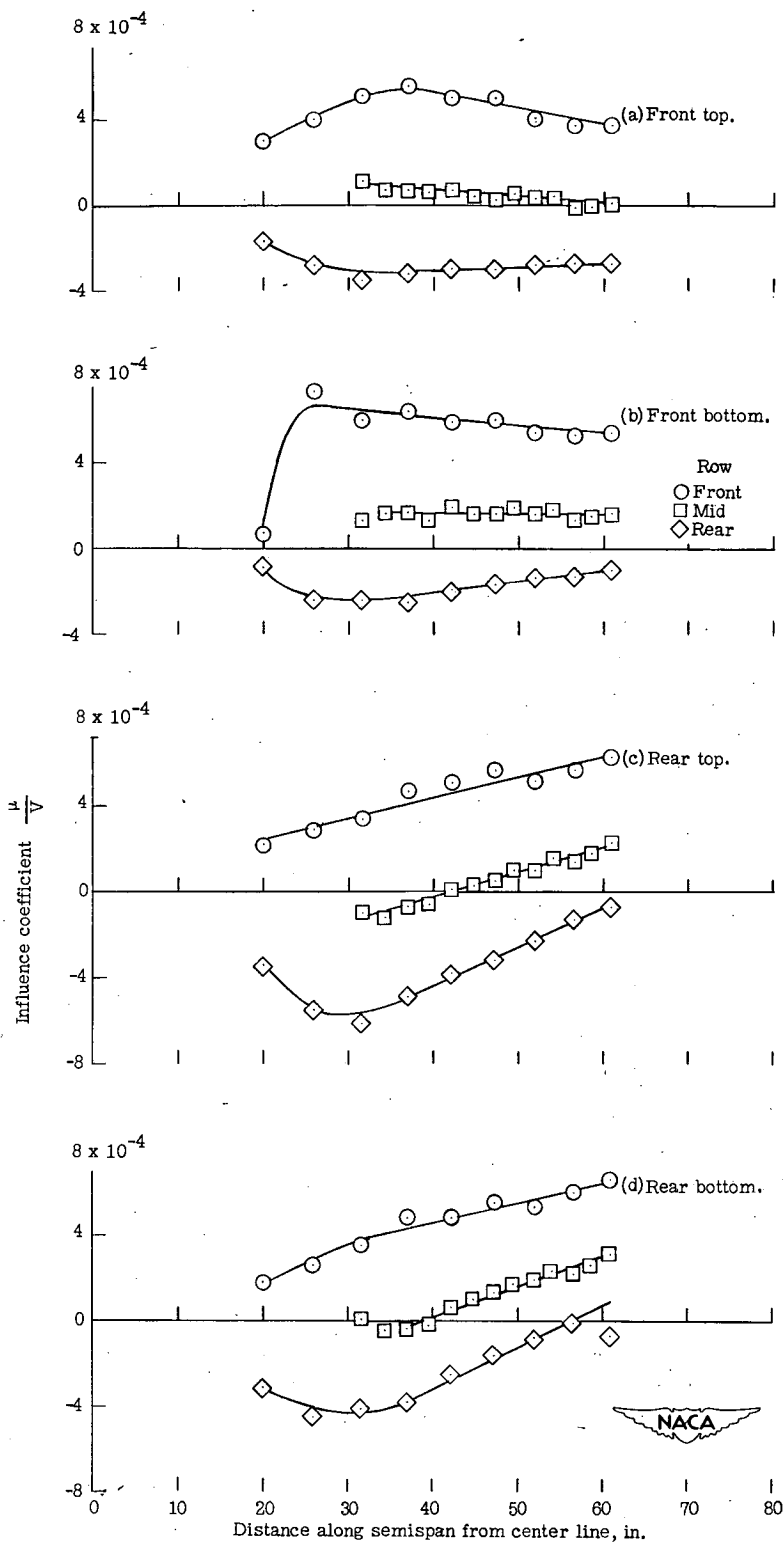


Figure 16.- Influence coefficients for structure B - uncombined left torque bridges.

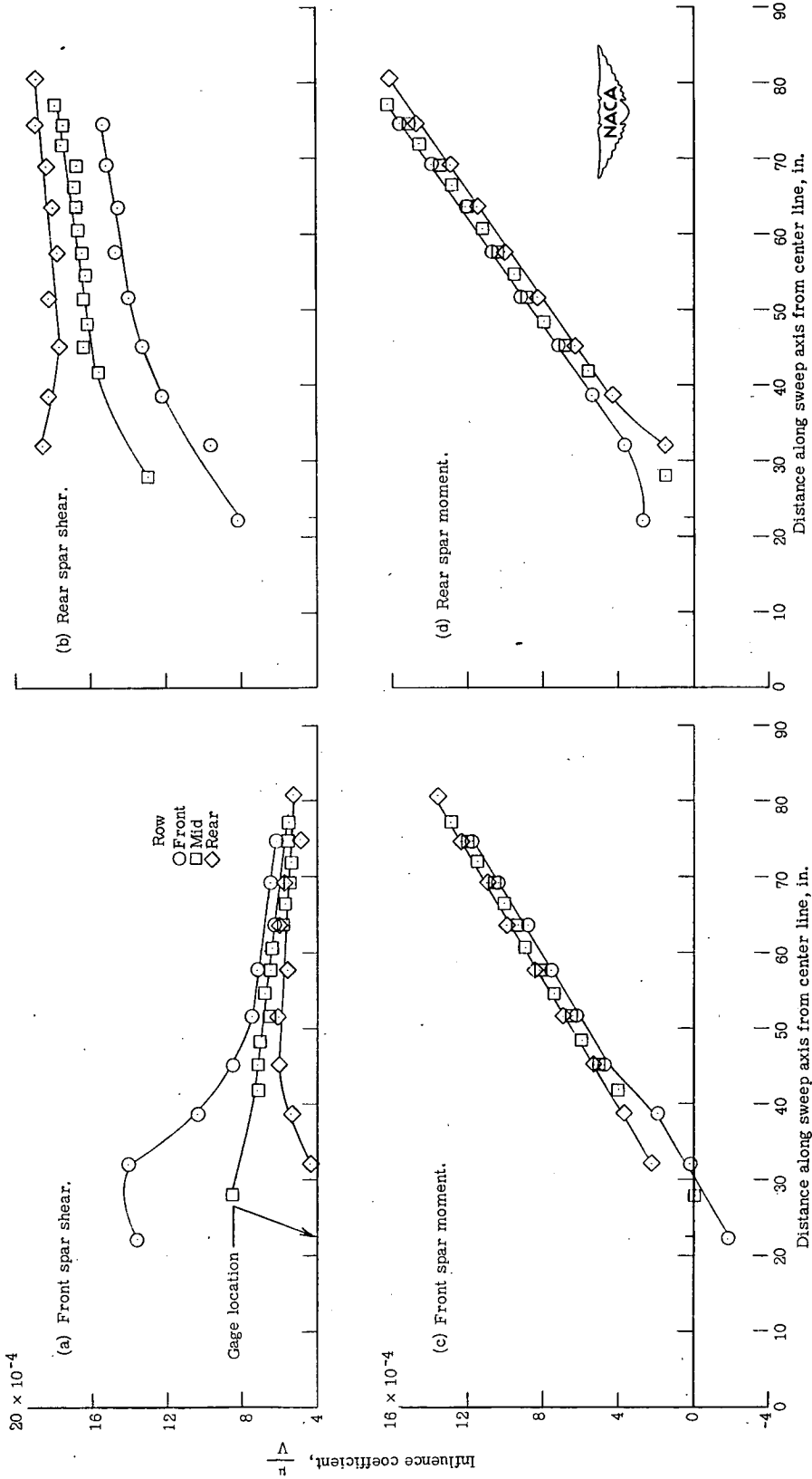


Figure 17.- Influence coefficients for structure B - uncombined left shear and moment bridges, gage station 2.

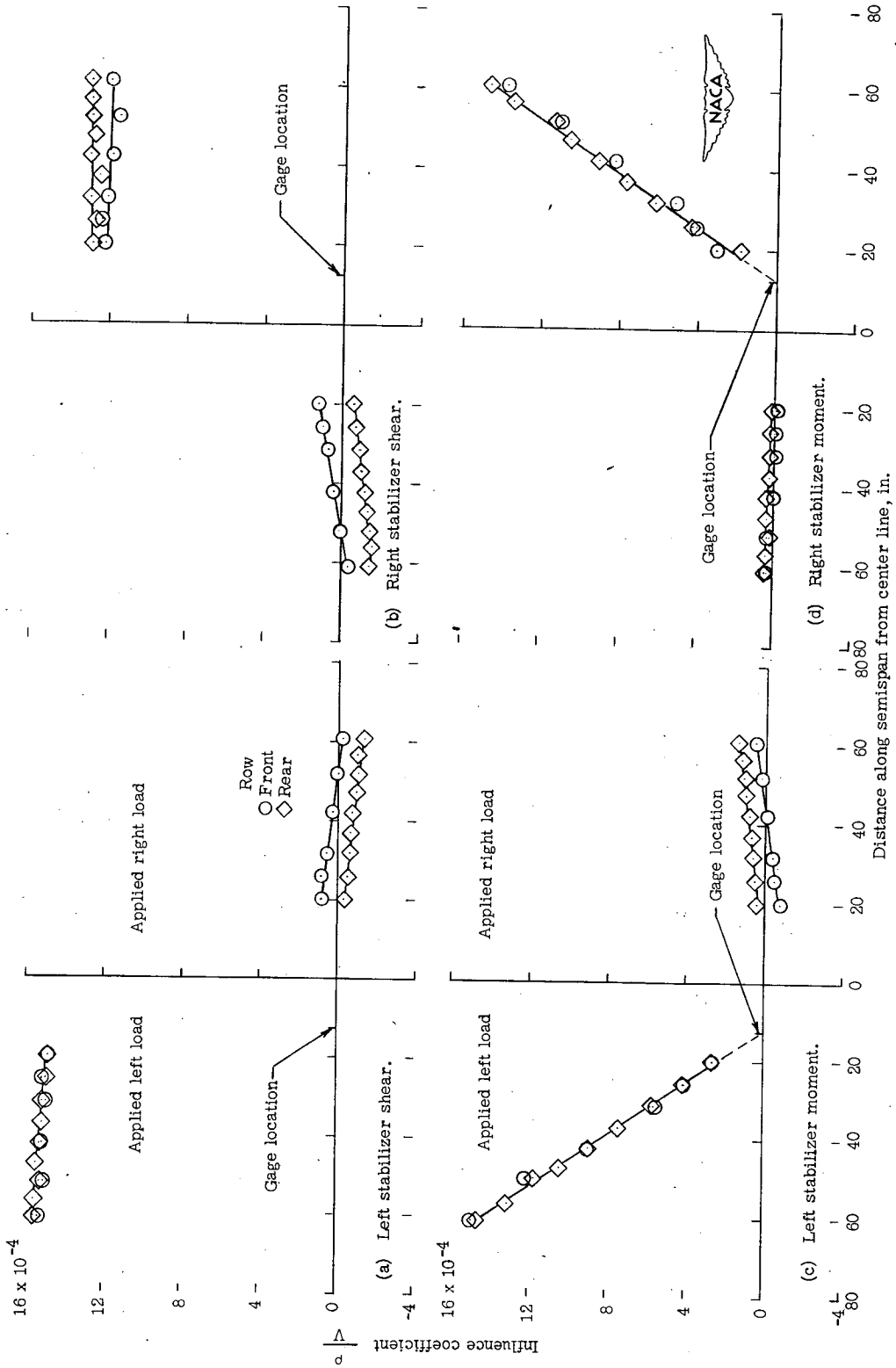


Figure 18.- Influence coefficients for structure B - combined bridges, gage station 1.

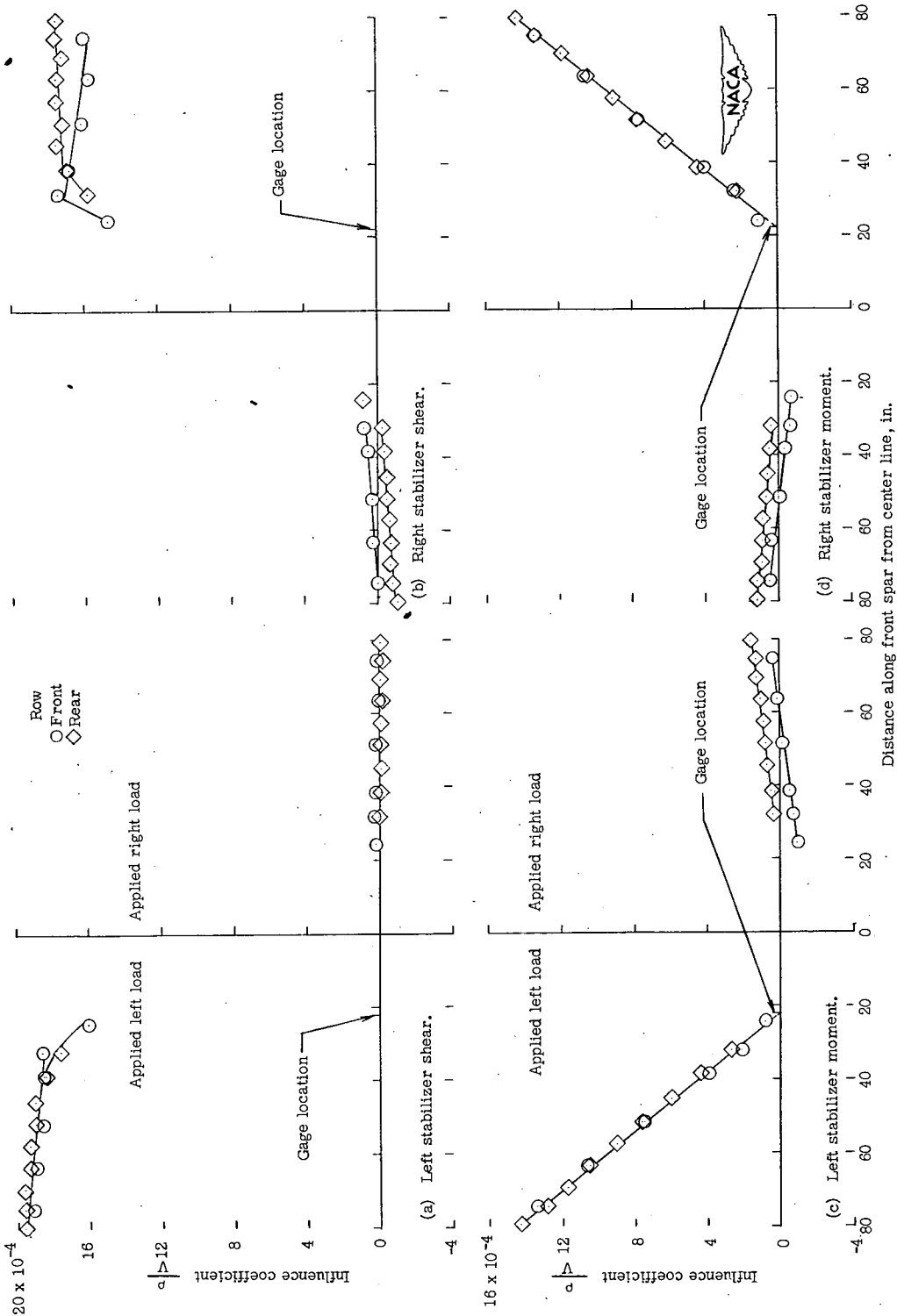


Figure 19.- Influence coefficients for structure B - combined bridges, gage station 2.

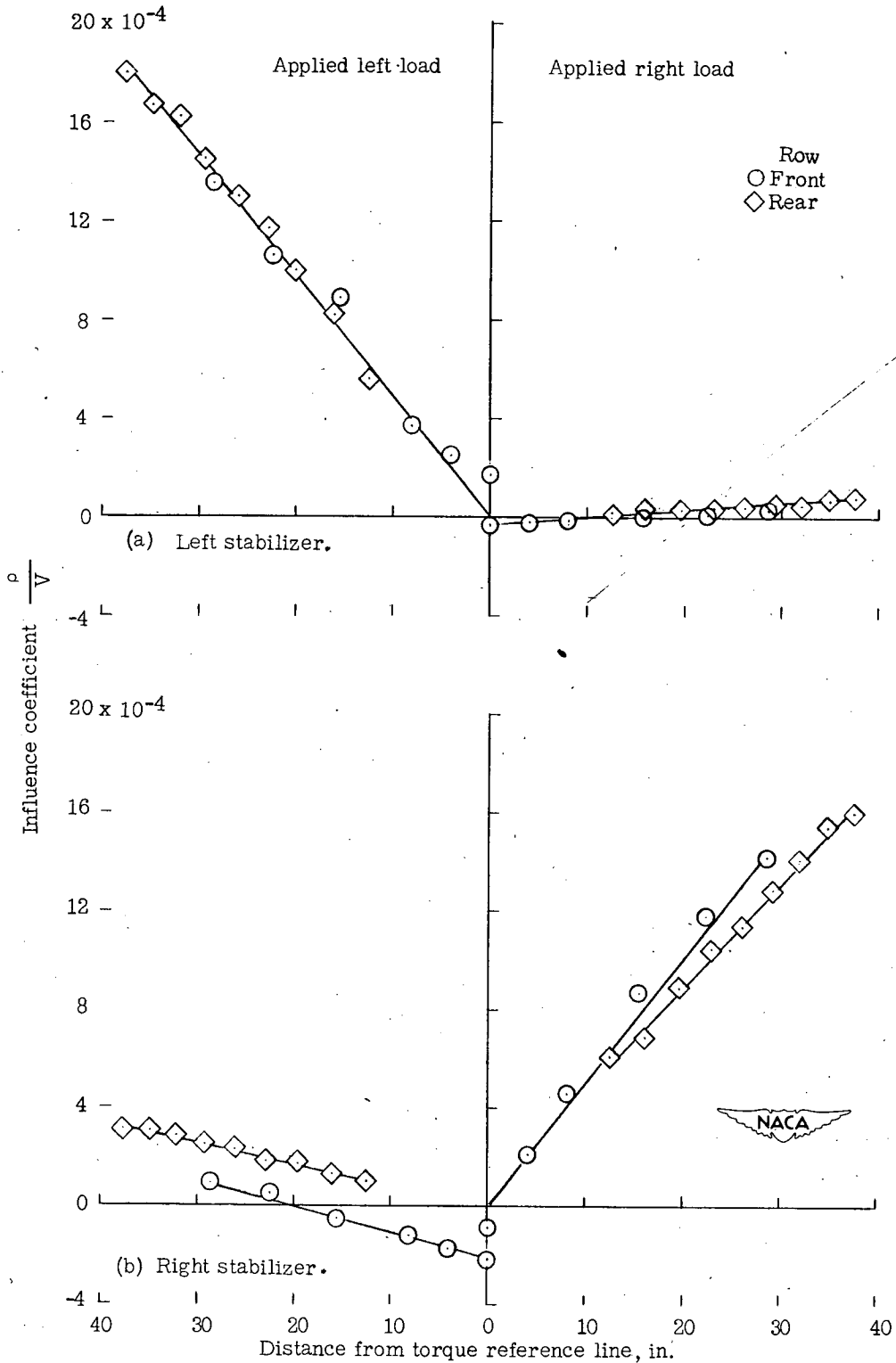


Figure 20.- Influence coefficients for structure B - combined torque bridges.

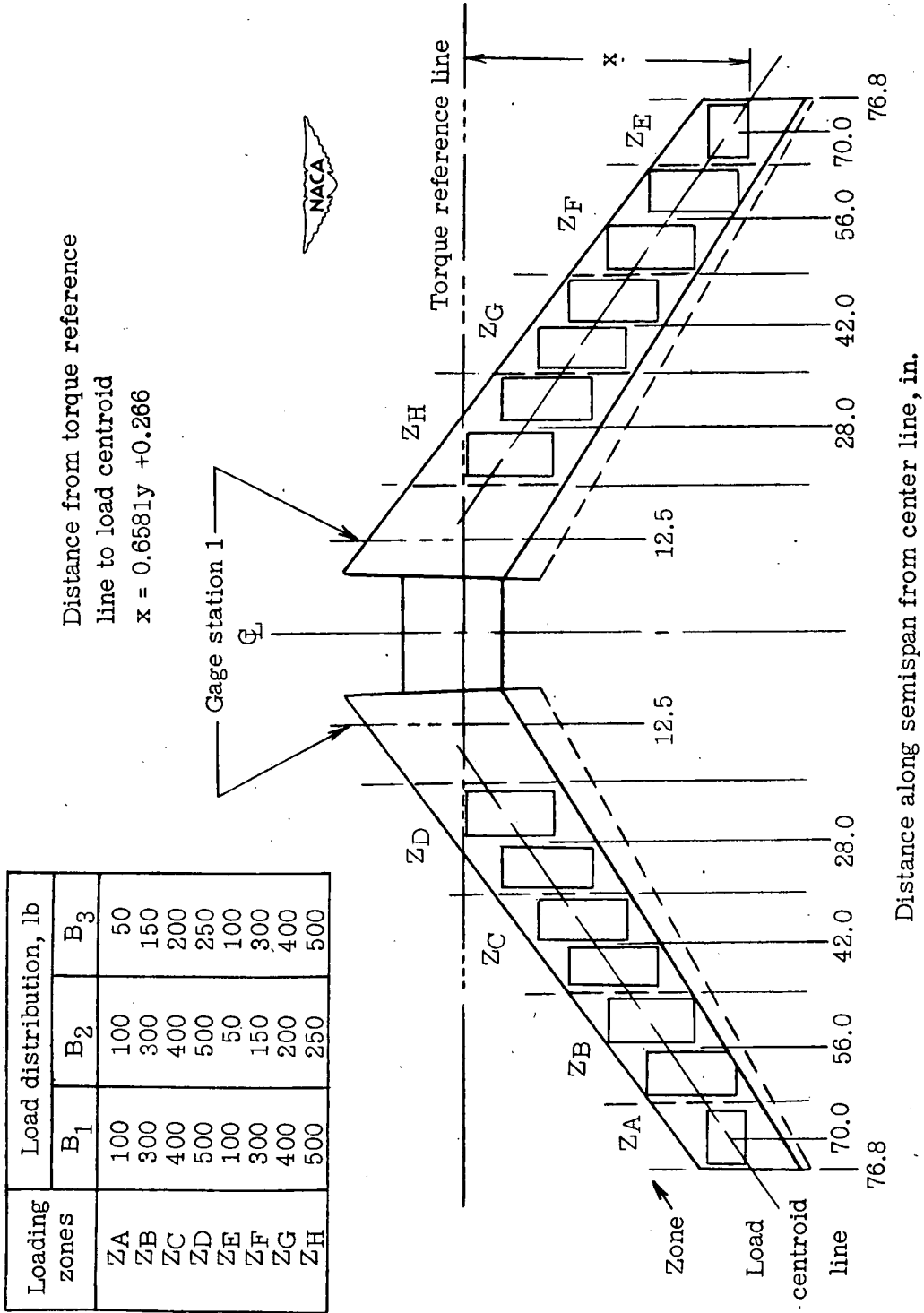


Figure 21.- Distributed check loads B₁ to B₃ applied on structure B.

SECURITY INFORMATION

~~CONFIDENTIAL~~

~~CONFIDENTIAL~~